LUND UNIVERSITY

Master of Science Thesis
VT2015

Accuracy of Quantification for Renography with 99mTc-MAG3: A Study on Virtual and Clinical Data

Irma Ceric

Supervision

Marie Sydoff, Jolanta Bartosik, Michael Ljungberg and Gustav Brolin

This work has been performed at
Dept of Clinical Physiology, Helsingborg Hospital, Helsingborg

Department of Medical Radiation Physics,
Clinical Sciences, Lund
Lund University

Contents

1 Popular Scientific Summary in Swedish

Funktionen hos kroppens reningsverk

Njurarna har en renande funktion i kroppen. De ser till att blodet är fritt från olika ämnen och att kroppen gör sig av med restprodukter. Dessutom producerar binjurarna hormoner och reglerar blodtrycket. Detta är bara några av de många egenskaper som njurarna har. Eftersom njurarna har en viktig roll i många processer i kroppen kan en nedsatt njurfunktion ha flera olika typer av symptom som trötthet, högt blodtryck och sämre aptit. För att få information om njurarnas funktion kan en så kallad renografi göras.

Vid en nuklearmedicinsk undersökning används ett läkemedel som märks med en radioaktiv isotop, ett så kallat radiofarmaka. Detta radiofarmaka injiceras i patienter för att undersöka funktionen av olika organ i kroppen. Beroende på vilket organ som önskas undersökas, används olika radioaktiva läkemedel. Efter injektionen tas bilder med en gammakamera, denna samlar in bilder dynamiskt (i en tidssekvens). Sammanlagt fås 84 bilder, varje bild består av ett antal pixlar och varje pixel har ett numeriskt värde som motsvarar de counts i bilden som motsvarar isotopupptaget. Vid utvärderingen definieras ett område; ett så kallat ”region of interest” (ROI) runt varje njure och värdena som fås i dessa ROI används för att uppskatta upptaget i njuren. Sedan görs även en korrektion för upptag i andra delar av kroppen, detta görs genom att lägga så kallade bakgrunds ROI som omgärdar njuren i bilden och som kan ritas på olika sätt. De värden som fås efter denna korrektion plottas sedan som en funktion av tiden. Sättet att utföra och utvärdera renografi kan variera från sjukhus till sjukhus trots att undersökningen funnits inom sjukvården under en längre tid. I denna studie har vi jämfört olika bakgrunds-ROI för att korrigera för aktivitetsupptag i bakgrunden. Vi har också utvecklat ett automatiserat sätt att lägga ROI runt njuren i bilden och jämfört detta med att lägga dem manuellt, vilket idag är standard på många sjukhus. Vi började med att göra en så kallad aktivitetskvantifiering med ett antropomorfiskt fantom. Det antropomorfa fantomet är gjort av plexiglas och efterliknar en del av överkroppen hos en människa, innehållande lever, njurar och en del av ryggraden. Organen är ihåliga och kan fyllas med vatten blandat med ett radioaktivt ämne. Genom att mäta aktiviteten innan bildtagning och beräkna aktiviteten utifrån bilderna kan en jämförelse mellan mätningen och beräkningen göras, för att besämma hur nära sanningen man kan komma. Vi har även använt oss av virtuellt framtagna datapatienter där vi på förhand definierat njurens funktion genom att i föröväg bestämma hur mycket av det radioaktiva ämnet som skall tas upp av njurarna. På så sätt har vi kunnat bestämma vilken korrektionsmetod och utvärderingsmetod som är bäst. Vi har därefter gjort en patientstudie på 25 patienter och i dessa bilder applicerat den bakgrunds-ROI som gav det bästa resultatet i bilderna från de virtuella patienterna.

Standardundersökningen görs med en detektor under patienten; vi har även undersökt om resultatet av utvärderingen blir bättre med ytterligare en detektor ovanför patienten vid bildtagningen (anterior= över och posterior= under). Bilder i anterior och posterior position används för att beräkna det sk. ge-

ometriska medelvärdet, vilket gör att uppskattningen av upptaget i njurarna blir oberoende av njurarnas placering (i djupled). Denna metod tar alltså hänsyn till njurens position vilket standardundersökningen inte gör.

Utifrån resultaten föreslår vi att ett geometriskt medelvärde ska beräknas på bilder från alla patienter, eftersom det finns en risk för över- eller underskattning av njurarnas funktion om insamlingen sker med endast en detektor under patienten. Studien har visat att då vi placerar bakgrunds-ROI en bit bort från njuren så får vi en mer korrekt beräkning av njurens funktion, framförallt för höger njure och då funktionen är nedsatt. Resultaten visar även att man kommer närmare de faktiska värdena på ett digitalt fantom om man lägger bakgrunds-ROI automatiskt jämfört med manuellt.

2 Abstract

Aim: Renography with ^{99m}Tc-MAG$_3$ is one of the most common nuclear medicine examinations. It's extensive use justifies a thorough investigation of the methods used to accurately determine the split renal function, for instance with regard to background subtraction and correction for renal depth differences. Previous studies on this subject have been made, mainly on patient image data, thus the "true" values have not been possible to determine. In this study, both patient images and images from virtual patients obtained from Monte Carlo simulations have been used in the analysis in order to determine the most accurate method for quantitating the split renal function.

Method: Initially, a transmission measurement was performed with a ^{57}Co flood source and an anthropomorfic phantom (KYOTO KAGAKU) filled with water. The phantom was then filled with an activity concentration corresponding to the uptake in a real patient and an activity quantification was performed. Additionaly, twenty sets of simulated dynamic renography images obtained from a gamma-camera simulation of an anthropomorphic digital XCAT phantom together with 25 dynamic patient studies were used for analysis. The split renal function was calculated from the images using three different types of ROIs for background correction; (a) distant perirenal ROI (2 pixels wide and 4 pixels outside the kidney ROI) (b) adjacent perirenal ROI (2 pixels wide and 1 pixel outside the kidney ROI) and (c) adjacent lateral ROI (2 pixels wide and 1 pixel outside the kidney ROI). Distant and adjacent perirenal ROIs were applied with an automated program, adjacent lateral ROI was both automatically and manually drawn. To determine which background correction method that gave the most accurate results, the kidney and the background ROIs were drawn in all simulated images with split renal functions ranging from 50-50% to 90-10%. The background ROI that gave the most accurate result in the simulated images was then used in a separate study to investigate the improvement of applying the geometrical-mean (GM) correction on anterior/posterior images from patient studies. The operator dependence was also studied by comparing results obtained with manually drawn and with automatically generated ROIs.

Results: The deviation from the true uptake values was smallest when using the distant perirenal ROI. The largest error was associated with the lateral ROI. The GM method, in contrast to assessment with solely posterior images, corrects for kidneys which are placed at different depths in the body. The use of automatically placed ROIs showed more reproducible results without the intra-operator variability.

Discussion: The use of virtual images in conjunction with patient studies was found to be very useful for estimating uncertainties associated with background correction, operator dependence and the use of the GM method. The method which was most accurate and hence suitable to use in clinical routine was the GM method with automatically drawn, distant perirenal background ROIs.

Conclusions: The result of this study supports the use of distant ROIs when calculating the split renal function, preferably applied with an automated

ROI program. The GM method is recommended as a standard method in the clinic.

3 Introduction

In addition to purging our bodies from toxins and waste, the kidneys have many essential functions; for instance regulation of water, electrolyte balance, blood pressure, calcium levels and levels of red blood cells. The kidneys and the urinary tract can be subject to various pathological conditions. When the renal function is degraded, the symptoms can be versatile and the examination form can vary.

One of the most essential calculations when performing renography is the split renal function, which is obtained by calculating the percentage contribution for each kidney of the total kidney function. When estimating the split renal function, renography is the primary choice [1]. This is done by intravenous injection of a radiopharmaceutical, for instance $^{99m}Tc - MAG_3$ (mercaptoacetyltriglycine). A dynamic dataset of images are then acquired with a gamma camera. The change in radiopharmaceutical concentration over time is used to evaluate renal function. According to a survey performed by EQUALIS[1] in 12 hospitals in Sweden, 3 631 people were examined with renography during the year of 2010, including adults and children [2].

The physiological processes associated with the renal-urologic system are imaged dynamically with a gamma camera. The radiopharmaceutical enables visualization of the uptake and excretion of the renal-urologic system. The change in radiopharmaceutical concentration over time is used to evaluate renal function. The split renal function shows values of the relative function of the kidneys. This means that even in cases in which both kidneys have a degraded function the sum of the split renal function will still add upp to 100 %. When an image has been acquired, regions of interest (ROIs) are drawn around the organ of interest and also adjacent to the organ of interest. The adjacent ROI is of importance when correcting for background activity (adjacent ROIs) and blood stream contribution (aortaROI). The standard method is to collect the data by registration of counts solely in the posterior view. This method is not the optimal choice of data collection since it is not possible to account for different depths of the kidneys. There are two accepted algorithms that can be used to calculate the split renal function: the integral method and the Patlak-Rutland method. A comparison of the two methods show that the integral method provides the best precision [4]. In this study, the integral method is used for calculating the split renal function. The integral method assumes that the kidneys are located at the same depth, but this is not always the case. By collecting data with an anterior and a posterior detector, the so-called conjugate view-method, and then calculating the geometric mean (GM), the results are not depth-dependent. [9].

There are different ways to perform a background correction. For example one can choose perirenal, elliptical or lateral ROIs. According to a study performed by Andrew Taylor *et al.*, background correction with elliptical and perirenal ROIs give more reproducible results that the lateral ROI method [5].

[1] EQUALIS is a non profitabel company providing schemes for external quality assessment to improve quality of diagnostic procedures as well as treatments in health care. Their main goal is to improve patient safety.

We wish to further investigate this conclusion by using the different ROIs for background correction in simulated images with a known split renal function. We have compared the estimations made with manually drawn ROIs used at the clinic in Helsingborg to the corresponding estimations made with automatically applied ROIs, for the simulated images (a program was created that automatically defines the ROIs (Appendix I)). Two different background ROIs were applied with the automated method. The evaluation process was divided into the following comparisons:

1. Manual adjacent lateral ROI and automated lateral adjacent background ROI for simulated images (posterior).

2. Automated adjacent lateral ROI, compared with two different background ROI; adjacent perirenal and distant perirenal ROI, for the simulated images (posterior).

3. The best method obtained from (1) and (2) was applied on the patient images.

4. GM in combination with transmission measurements was applied on the patient data.

The split and total renal function in combination with other relevant information about the patient was used in the evaluation and decision making of further medical care. To obtain a reliable and reproducible technique and to ensure the best possible care for the patients as well as equal performance and interpretation of the renogram among various centers, the use of a more accurate method is desirable [6]. Radioisotope studies of the kidneys are a common examination form and is used as a standard procedure at many clinics since its first description in 1956 [7]. A difference in assessment has been observed between different clinics. The European Association of Nuclear Medicine (EANM, 2011) have published guidelines for standard and diuretic renograms in children. Since no similar guidelines for adults have been published, a difficulty emerges when comparing studies and results performed at different clinics. The participation of Helsingborgs general hospital in the 2010 EQUALIS survey showed deviations in the results for two phantom measurements. For this reason an evaluation of the assessment method used, was desired.

The aim of this study was to compare the positioning of ROIs used for background correction, as made at Helsingborgs general hospital, manual adjecent lateral ROIs, with three different ways of automatic placement of background ROIs (adjacent lateral background ROIs, adjacent perirenal background ROIs and distant perirenal background ROI). This was made with Monte Carlo simulated image data. The simulated images offer a possibility to compare how the placement of the background ROI affect the result, i.e. the split renal function. The background ROI method which yielded the smallest deviation from the known split renal function in the simulated images, was applied on patient images from 25 patients. The evaluation was performed on solely posterior view images, anterior and posterior view images (GM) and GM in combination with transmission measurements for the patient images. Finally, it was investigated how the split renal function is affected when the evaluation is manually per-

formed compared to the automatically performed assessment.

4 Theory

4.1 Absolute Measurement of Activity

The standard method when performing renography is to acquire images with one camera head posterior of the patient. Alternatively one can use two detector heads, one placed in anterior view and the other in posterior view of the patient; this is the so called conjugate view method. The conjugate view method allows for calculation of the geometric mean. By doing so one can more precisely determine the absolute activity as well as the absolute renal function. The calculation of the absolute activity presented in this section, is based on a measurement performed on a phantom with a cross sectional area enclosing a rod. The rod is filled with an activity solution and is positioned perpendicular to the detectors field of view (figure 1) [8], i.e. from the detector FOV only a cross-section of the rod is observed, dx in figure 1.

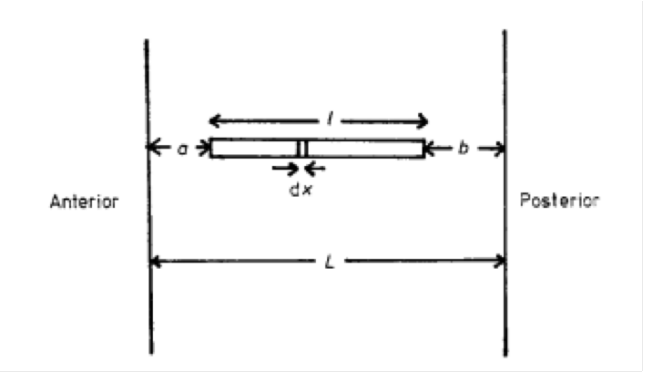

Figure 1: Illustration of the phantom used in the measurements [1].

The relationship to obtain the count rate for the anterior, R_A, and posterior view, R_P, is given by the expression in equation 1 and 2.

$$R_A = E \cdot A \cdot e^{-\mu_1 a} \int_0^1 e^{-\mu_2 x} dx = \frac{EAe^{-\mu_1 a}}{\mu_2}[1 - e^{-\mu_2 l}] \tag{1}$$

$$R_P = E \cdot A \cdot e^{-\mu_1 b} \int_0^1 e^{-\mu_2 x} dx = \frac{EAe^{-\mu_1 b}}{\mu_2}[1 - e^{-\mu_2 l}] \tag{2}$$

Where A is the activity concentration μCi/ml in the rod, E is the sensitivity of the gamma camera, a is the distance from the phantom/patient surface to the position of the rod for the anterior view b is the corresponding distance for the posterior view and l is the source length. μ_i is the linear attenuation coefficient for the rod and for the tissue respectively.

$$(R_A \cdot R_P)^{1/2} = \frac{EAe^{-\mu_1 (a+b)/2}}{\mu_2}[1 - e^{-\mu_2 l}] \tag{3}$$

A first order attenuation correction can be made by multiplying the geometric mean (equation 3) with $e^{\mu_2 l/2} e^{\mu_1 (a+b)/2}$. This gives a corrected geometric mean count rate, R_{GM}, (equation 6).

$$R_{GM} = (R_A \cdot R_P)^{1/2} \cdot e^{\mu_2 l/2} e^{\mu_1 (a+b)/2} = \frac{E \cdot A}{\mu_2} \left(e^{\mu_2 l/2} - e^{-\mu_2 l/2} \right) \tag{4}$$

The expression in equation 4 can be rewritten by substituting the hyperbolic definition:

$$sinh(x) = \frac{e^x - e^{-x}}{2} \tag{5}$$

Which yields

$$R_{GM} = \frac{E \cdot A \cdot l \cdot sinh(\mu_2 l/2)}{\mu_2 \cdot 2 \cdot l} \tag{6}$$

If the linear attenuation coefficient, μ, of the tissue and the source containing the activity are equal, which is the case in patients, the attenuation can be rewritten according to equation 7.

$$e^{\mu l/2 + \mu(a+b)/2} = e^{\mu(l+a+b)/2} \tag{7}$$

Next, the obtained expression is divided with the efficiency of the detector E, which can be seen in equation 8. The true activity Al expressed in equation 9 can then be calculated.

$$\frac{(R_a + R_P)^{1/2} \cdot e^{\mu(l+a+b)/2}}{E} = \frac{Al \sinh(\mu l/2)}{2\mu l} \tag{8}$$

$$Al = \frac{(R_A \cdot R_P)^{1/2}}{\left[\frac{sinh(\mu l/2)}{\mu l 2} \cdot e^{-\mu(l+a+b)/2} \right] \cdot E} \tag{9}$$

This expression was first derived by Fleming in 1979 [8].

4.2 Transmission Measurement

In order to determine the attenuation correction factor,$e^{-\mu(l+a+b)/2} = e^{-\mu \cdot T/2}$, where $T = l + a + b$ in equation 9, transmission measurements with an external source can be performed. Registration of a blank measurement (no patient, R_0), and a transmission measurement (with patient, R) with an external source, prior to the administration of the radiopharmaceutical enables the correction. The ratio of the blank and the transmission measurements gives the attenuation correction factor (equation 10).

$$\frac{R}{R_0} = e^{-\mu \cdot T/2} \tag{10}$$

The transmission measurements are performed with a ^{57}Co flood source. Since the photons from ^{57}Co does not have the same energy and thus not the

same attenuation coefficient as ^{99m}Tc, which is used during the examination, this needs to be corrected for. The effective attenuation coefficient is then:

$$\frac{R}{R_0} = e^{-\mu_{eff}T} \Rightarrow \mu_{eff} = \frac{-R/R_0}{T} \tag{11}$$

Where R_0 is the blank registration, R is the registration with the phantom on the couch. The effective attenuation coefficient, μ_{eff}, was further rescaled.

$$\mu_{eff}^{Y} = \frac{(\frac{\mu}{\rho})Y \cdot \mu_{eff,X}}{(\frac{\mu}{\rho})X} \tag{12}$$

Where X is the radionuclide that the transmission measurements were performed with and Y is the radionuclide with which the emission measurements were done.

4.3 Background Correction

When correcting for background activity in nuclear medicine images, ROIs are drawn around the organs of interest. The counts registered in the organ ROIs can be affected by overlying and underlying organs who's activity contributes by adding unwanted counts to the ROI value. This can result in misleading information about the uptake of activity in the organ of interest. To correct for this, additional ROIs can be placed in close proximity to the organ ROIs; so-called background ROIs. The number of counts per pixel in the background ROI is then multiplied by the number of pixels in the organ ROI. This value is then subtracted from the number of counts in the organ ROI. There are different ways to perform background correction. As an example, we present two methods; the Gates and the Kojima method.

Gates background correction method is the so-called 'conventional' background correction method: the count rate in an adjacent ROI is subtracted from the count rate in the kidney ROI. This is expressed as:

$$R'_P = R_P - R_{P,bcg} \tag{13}$$

$$R'_A = R_A - R_{A,bcg} \tag{14}$$

where R'_P and R'_A is the corrected count rate in the anterior and the posterior image, R_P and R_A is the count rate measured at the source area with one detector head in posterior and anterior view and $R_{A,bcg}$ and $R_{P,bcg}$ is the background count rate [11,12]. This method may overestimate the background activity, and thus could underestimate the uptake of activity in the kidneys since neither the thickness of the kidneys nor the thickness of the patient is taken into account.

The Kojima background correction method accounts for kidney and body thickness [13]. The mathematical relation can be expressed as:

$$R'_A = R_A - R_{A,bcg} \cdot C_A \tag{15}$$

$$R'_P = R_P - I_{R,bcg} \cdot C_P \tag{16}$$

Where

$$C_A = 1 - \frac{e^{\mu(T-a-t)} \cdot [1 - e^{-\mu t}]}{1 - e^{-\mu T}} \tag{17}$$

and

$$C_P = 1 - \frac{e^{\mu b} \cdot [1 - e^{-\mu t}]}{1 - e^{-\mu T}} \tag{18}$$

Where t is the effective thickness of the kidney, T is the body thickness, b is the kidney depth from the posterior view and and a is the kidney depth from the anterior view. μ is the narrow beam linear attenuation coefficient, equal to 0.15 cm^{-1} for ^{99m}Tc.

The choice of background correction method is proven to affect the estimation of the split renal function in several published studies [14,15,5]. Even though a multiple of presented methods are available, many are not applicable in clinical context. For example, in order to use the Kojima correction method the depth and thickness of the kidneys must be known. This in turn requires additional imaging which is time consuming. Due to this, the conventional Gates method is often used even though it is not the optimal choice. In addition, the positioning of the background ROI is believed to affect the estimation of the split renal function.

Extra- and intra-renal activity is corrected in the background subtraction techniques used at many hospitals. The extra-renal activity includes the filtration of the activity in the kidneys, the blood activity in the kidneys and extravascular activity in the kidneys. The extra-renal activity is obtained from organs close to and around the kidney and is due to blood activity and extravascular activity. To obtain a correct calculation of the kidney function only the filtration of activity should be included and the remaining components of the extra- and intra-renal activity should be corrected for [1]. To determine the proportion of the count rate due to background activity is hard to estimate. If corrections are performed poorly they can have an unwanted effect on the calculation of the split renal function. Two background ROIs are used to correct for extra- and intra -renal activity; an aorta ROI corrects for intra-renal activity and a ROI surrounding the kidney corrects for extra-renal activity. A perirenal ROI slightly separated from the kidney to avoid incidence of scatter is recommended by the International Scientific Committee of Radionuclides in Nephro-Urology [16].

4.4 Renal Anatomy and Physiology

The kidneys are components of the renal-urologic system. In addition to the kidneys, two ureters, a bladder and the urethra make up the renal-urologic system. They are positioned on the abdominal wall retroperitoneal to the organs of digestion. The position is on both sides of the spinal column, outside the

12th thoracic and third lumbar vertebrae, Th12-L3, see figure 2 (Henry Gray 1918:20). Each kidney is normally bean shaped and encased in a renal capsule with an approximate size of 11 by 7 cm and a thickness of approximately 3 cm [17].

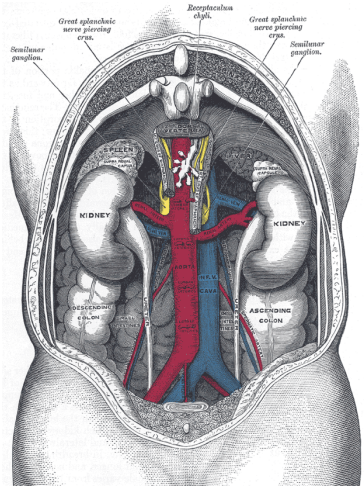

Figure 2: The location of and environment surrounding the kidneys (Henry Gray 1918:20) [2].

On top of each kidney,the adrenal glands are positioned (figure [2]). These are responsible for the production of the hormones aldosterone, cortisone and androgens (Henry Gray 1918:20). On the medial side of each kidney there is an opening, hilum, which enables the renal artery and vein to enter the kidneys as well as the ureters to exit the kidneys. The processes taking place in the kidneys can roughly be divided into two main groups: the excretion of urine and the filtering of the blood. The internal structure of the kidneys consist of an outer cortex which encloses the inner medulla. The inner medulla consists of a number of triangular shaped pyramids in which the nephrons lie, approximately 1,2 million in each kidney[17,18]. The nephrons are the functional units of the kidneys.

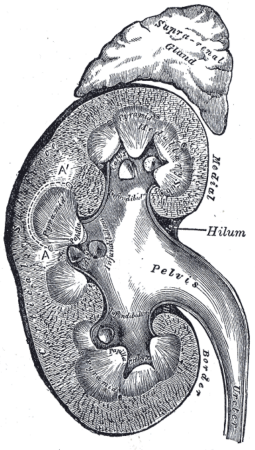

Figure 3: The general anatomy of the kidneys, vertical slice (Henry Gray 1918:20) [3].

The nephrons have a cup-like structure, the Bowman's capsule, in which the glumeruli sits, a network of capillaries. The Bowman's capsule and the glumeruli form the renal corpuscle. The nephrons are the kidneys functional unit and here the primary urin is formed. The primary urin flows through the proximal convolute tubule which exceeds into the loop of Henle and further on into the distal convoluted tubules.The urine is drained into the collecting ducts which merge to form renal papilla. The urin is further drained into the major and minor calyces and from the calyces to the renal pelvis and exits the kidneys through the ureter to the bladder.

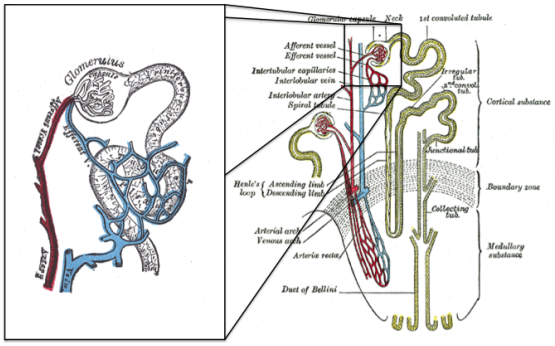

Figure 4: The renal tubuli scheme and enlarged Bowman's capsule and glumerulus (Henry Gray 1918:20) [4].

The blood flows to the kidneys via the left and right renal artery. The arteries branch further inside the kidneys to the so-called arterioles. When entering the kidneys the blood is of high pressure and it flows into knots of vessels, the glomeruli. The glomeruli and the capsule membrane contains pores. These pores are able to filter the blood from water and substances into the nephron. Here the blood pressure drops and the blood floats into arterioles, which are connected to small veins. These small veins are further reunited and form the renal veins. The blood is then returned to the inferior vena cava and further into the heart. Every day approximately 1 500 liters of blood passes through the arteries of the kidneys. 20% of this is filtered in the glomerulus and form the primary urine, which is passed through the tubules and is reabsorbed so that the net urine makes up 1% of the primary urine.

The kidneys play an essential role in maintaining the internal environment, homeostasis, in the body, by regulating the extracellular fluid, ECF, (interstitial fluid and plasma) and intracellular body fluid, ICF, (fluid within the cells). The regulation of osmolality also contributes to maintaining homeostasis, where osmosis means the transport of water across the semipermeable cell membrane. This transport occurs when the concentration of ions differs on both sides of the membrane [18]. The goal when regulating ECF and ICF as well as osmolality is to keep the fluid constant in order to keep the cells alive. The regulation occurs via renal excretion of sodium (Na^+), chloride (Cl^-) and water (H_2O) but also by eliminating the protein waste product, urea [19]. Releasing the hormone aldosterone, produced in the adrenal glands, regulates the body supply of sodium, chloride and water. The stable salt and water balance result in stable blood volume and pressure. The salts in the body consist of different types of ions. When the salts dissolve in the body electrically conductive ions are produced; electrolytes, anions and cations. The excretion through the kidneys, regulate the amount of the different electrolytes, obtaining equilibrium. The kidneys also regulate the acid-base balance in the body. Substances that are water-soluble and emit protons are called acids and substances that intercept

protons are called bases. The kidneys role in the acid/base balance is to excrete acid in the form of hydrogen (H^+) ions.

4.5 Dynamic Imaging

Planar gamma camera imaging can, as mentioned, be used to image physiological processes in the body. A pharmaceutical is labelled with a radionuclide, forming a radiopharmaceutical which can be used in imaging of various functions in the body. After intravenous injection, the radiopharmaceutical participates in physiological processes in the body. The radionuclide emits gamma rays which is detected by the detectors in the gamma camera forming images of the distribution of the radiopharmaceutical in the body. The most frequently used radiopharmaceutical for renography is ^{99m}Tc labelled with MAG_3. MAG_3 has a high renal extraction which yields good signal-to-noise ratio, SNR, and high concentration of the isotope in the urine. This is of advantage when diagnosing urological issues like obstruction and dilation in the urinary tract as well as reduced renal function [1]. Renography is used to determine split renal function when the medical issue is unilateral disease or obstructive nephropathies and as a part of the investigation before kidney donation. Because of this a reproducible method is desired so that small changes in the relative function of the kidneys can be diagnosed [1]. Traditional methods only use the posterior gamma camera head. By using two camera heads we enable calculations of the geometric mean of the counts in the two images, which makes the result independent of the kidney depth. During the examination, the patients lie in the supine position. EANM guidelines for diuretic renogram in children recommend that the image collection should be performed by using 10 s frames and consensus on split renal function recommend 10-20 s frames [15,16]. The minimal duration of the examination is set to 20 min with a matrix size of 128x128 pixels.

The choice of collimator affects the image and the choice of collimator depend on the tracer energy as well as the organ size. The collimators used for renography are parrallell hole collimators, such as low energy general purpose (LEGP) and low energy high resolution (LEHR) collimators. The collimator consistsis of an array of hexagonal channels and septa and they are often made of heavy materials such as lead. The channels enables only photons that travel perpendicular to the detector surface to pass through and contribute to form the image. When varying the width and length of the holes, the image resolution and sensitivity can be varied [21]. Generally, better spatial resolution yields reduced sensitivity. LEHR has a good resolution because of narrow holes and for the LEGP the hole diameter is larger which gives better sensitivity. When acquiring renograms the LEGP is often the best choice since a high count rate is more important than high resolution images. A scintillation crystal is used to detect the gamma rays that pass through the collimator. The gamma rays interact with the scintillation crystal which in turn emit scintillation light that is amplified in photomultiplier tubes. The signal is then converted into an electrical signal and digitalized to estimate spatial coordinates of the signal to form the image [20,21].

4.6 ^{99m}Tc mercaptoacetyltriglycin (MAG_3)

^{99m}Tc is a decay product of ^{99}Mo. One way to produce ^{99}Mo is by bombarding ^{235}U with slow neutrons. Several fission fragments are produced among these ^{99}Mo. To produce carrier-free radionuclides, the fission products are chemically treated. By washing the column with nitric acid the fission products are removed and ^{99m}Tc is left [21]. After production, the molybdenum is placed in a radionuclide generator and is sent to the hospitals where the ^{99m}Tc can be aqcuired by elution [20]. The principle of the generator is to isolate the short-lived daughter nuclide ^{99m}Tc from its longer-lived parent nuclide ^{99}Mo to obtain high radiochemical purity of the ^{99m}Tc. Because the daughter and mother nuclide have different chemical properties, the separation process is enabled. The different products binds with various strength to an aluminium (Al_2O_3) column. Positively charged aluminium ions absorb negatively charged molybdenum ions. At the hospital ^{99m}Tc is further labelled with MAG_3.

Several radiopharmaceuticals are available when performing renography. These highlight specific sub functions of the kidneys and can be catergorized into two groups depending on their extraction from the kidneys. Those extracted by glumerular filtration for example Tc-99m diethyenetriaminepentaaceticacid, DTPA. And those that are extracted by tubular secretion which is the case for ^{99m}Tc MAG_3 [22].

After intravenouse administration MAG_3 is bound to the plasma protein which keeps the radiopharmaceutical in the intravascular compartment. And thus blood pool activity in the heart, liver and spleen is prominent in the early images. The extraction fraction is 40 to 50 % which is defined as the fraction of cursor that disappears when the blood passes the kidneys vascular bed [1]. The chemical structure of ^{99m}Tc is shown in figure 5.

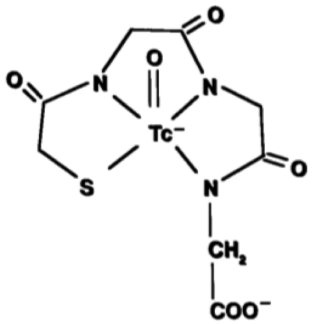

Figure 5: Chemical structure of ^{99m}Tc-MAG_3.

^{99m}Tc-MAG_3 is mostly cleared from the kidneys via the proximal renal tubules. The efficient extraction fraction of ^{99m}Tc-MAG_3 makes it suitable for determining renal function and thus makes it one of the primary used substances when acquiring renograms [23].

4.7 Image Evaluation

Evaluation of the acquired patient images from the renography can be performed by manually or automatically drawing ROIs. This is done for the left and right kidney and for the left and right kidney background. Manually drawn ROI induce inter- and intra-operator variability. The variability affects the resulting split renal function, especially when placing the background ROI at different positions. Choosing the optimal ROI for background subtraction is crucial and can easily over-or underestimate the kidney function. To be able to implement the assessment methods in the clinical environment the background correction as well as the ROI extraction has to be reasonably accurate and easily performed. Border detection of the kidneys is harder to distinguish when the kidney function is reduced. This is due to high background activity particularly in the liver and low kidney to background ratio.

The change in radiopharmaceutical concentration over time is used to evaluate renal function. The counts extracted from the chosen renal, aorta and background ROIs are plotted as Time Activity Curves (TACs). The curve show counts in ROI over time where the three phases (1) vascular phase, (2) the uptake phase and (3) the excretion phase can be distinguished [21] (see figure 6).

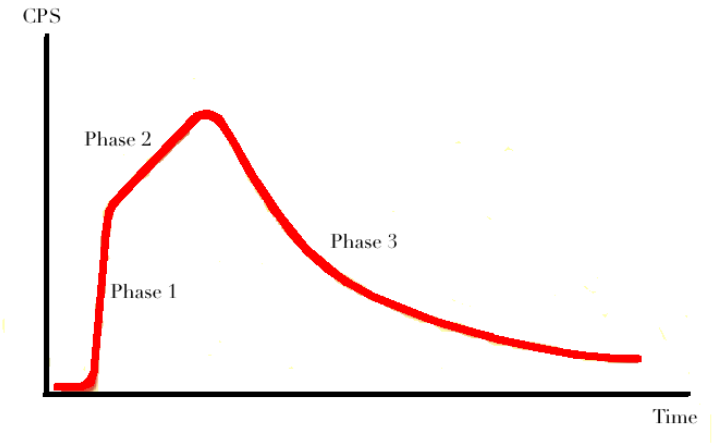

Figure 6: The different phases of the TAC, the vascular phase (phase 1), the uptake phase (phase 2) and the excretion phase (phase 3) [6].

The vascular phase in the renogram illustrates the tracers arrival at the bed of the capillaries, which indicates the speed and the vascular supply to the kidney. This gives a rapid raise in the renogram [1]. The uptake phase characterizes the kidneys ability to extract the radiopharmaceutical from the blood. The slope is dependent of the kidney function; the steeper the slope, the better renal function. The uptake phase lasts for 2-3 min up to 5 min before the excretion. During the uptake phase the curve reaches it's maximum value and exceeds into the excretion phase.The excretion phase represents the disappearance of the radiopharmaceutical from the kidney. In a normal functioning kidney the excretion starts 2-5 minutes post injection.

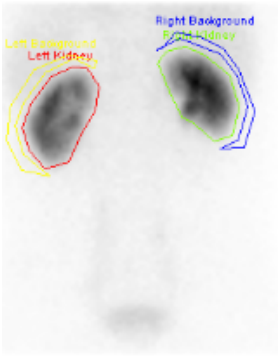

Figure 7: Shows positioning of renal ROI, adjacent lateral background ROI and aorta ROI which are essential for obtaining an accurate split renal function. Kidney and background ROIs are drawn manually whereas the aorta ROI is placed automatically and can be adjusted manually.

While recording the renogram, the counts during the phases mentioned above are registered. The registration exceeds beyond the wanted phases and collect unwanted counts from under- and overlying organs as well as the aorta. To correct for counts originating from over- and underlying organs as well as from activity in the aorta, background ROIs are drawn and these counts are subtracted from the number of counts in the kidney ROIs. By visually examining the TAC it can be established if the background activity and activity in aorta is correctly subtracted. When a correct subtraction has been made, the renography curve should start smoothly from zero.

To be able to correctly evaluate the renogram one needs to fully understand the examination. Both the physiological processes that takes place in the kidneys and the factors affecting the images. Therefore it is important to discuss and understand the underlying pitfalls of renography. Since the split renal function gives the relative function of the kidneys, the total sum of the split renal function will add up to 100 %. Thus the information about the global renal function is limited. Estimation of interval during which the split renal function is calculated can also affect the calculation of the relative function. The calculation of the split renal function should be performed before the excretion starts. The excretion to the pelvis occurs before the peak of the TAC start falling. Time to the peak is often used as guidance to set the stop criteria by visually examining the TAC. In many clinics the time is fixed to 2-3 minutes [6,24]. The risk of calculating a misleading split function increases if the excretion to the pelvis is included in the time chosen for the calculation since the total number of counts in the kidneys decrease after the extraction starts. The calculations used to determine the split renal function is based on the assumption that the calculation is performed during the uptake phase. Kidney depth can also affect the result and evaluation of the split renal function, therefore when depth difference is stated the evaluation should be performed with caution. Small differences in kidney depth can have a large effect on the resultant split renal function [1].

Depth determination could pose a problem and thus it needs to be corrected for. Correction for depth differences between the kidneys can be done by registration of a lateral image (where the distance between the kidneys and the detector is determined and used in combination with the attenuation correction factor) or geometric mean correction with anterior and posterior registration. The normal range of the split renal function is 45-55 % [6,15]. However, when concluding a statement about a patients renal function the whole clinical context needs to be taken into consideration.

4.8 Calculation of Split Renal Function

The split renal function can be derived from the concept of clearance which is given from Frick's principle. Frick's principle states that the amount of radiopharmaceutical that is eliminated from the plasma during passage of the organ is absorbed by the organ. There are three methods used for calculation of the split renal function. The integral method, the slope method and the Ruthland-Patlak method. The integral method has been shown to provide the most reproducible results and greatest precision, also lowest mean error induced by noise in comparison to Ruthland-Patlak and the slope method [25]. Only the integral method will be discussed in this study since the calculations are done according to the integral method. The integral method is only valid if calculated during the uptake phase. So it is of great importance to set an accurate starting and stopping point for the calculation, otherwise the kidney function can be underestimated [6]. The starting point is set to 1 minute after injection of the radiotracer and the endpoint should be set to 30 s before the peak since it is assumed that the excretion starts a few seconds before maximum [26].

If the plasma flow, F_p [ml/min], and the concentration of the plasma in the artery, c_a [MBq/ml], and vein, c_v [MBq/ml], is known, the activity over time in the organ can be given by equation 19.

$$\frac{dA_{org}}{dt} = F_p \cdot (c_a - c_b) \tag{19}$$

By multiplying the volume of the blood plasma,(PV), with the activity concentration in the plasma, (C_p), the change in plasma activity can also be expressed as equation 20.

$$\frac{dA_p}{dt} = -PV \cdot \frac{dC_p}{dt} \tag{20}$$

By assuming that only the organ we wish to determine the plasma flow in, accumulates the activity, equation 19 and 20 can be set equal to each other:

$$F_p(c_v - c_v) = -PV \cdot \frac{dC_p}{dt} \tag{21}$$

In order to have a mathematical relationship that corresponds to that of a human, the excretion of the tracer in the organ needs to be included; $E = (c_v + c_a)/c_a$.

$$F_p(c_a - c_v) \cdot E = -PV \cdot \frac{dC_p}{dt} \Rightarrow \frac{dC_p}{dt} = \frac{F_p(c_a - c_v) \cdot E}{-PV} \tag{22}$$

By assuming that the activity concentration in the artery, c_a, at an arbitrary time is equal to the mean activity concentration in the plasma at the same time, C_p, we obtain the relationship given in equation 23.

$$\frac{dC_p}{dt} = \frac{F_p \cdot E}{-PV} \cdot C_p \tag{23}$$

Solving the differential equation in 23 gives:

$$C_p(t) = C_{p,0} e^{-(F_p \cdot E/PV) \cdot t} \tag{24}$$

where $C_{p,0}$ is the plasma concentration of the tracer at time 0. Equation 24 shows a monoexponential function. To determine the area under the curve, an integration can be done:

$$C_p(t) = \int_0^\infty C_{p,0} e^{-(F_p \cdot E/PV) \cdot t} = C_{p,0} \left[\frac{e^{-(F_p \cdot E/PV) \cdot t}}{-F_P \cdot E/PV} \right]_0^\infty$$

$$= \frac{C_{p,0}}{F_p \cdot E/PV} \tag{25}$$

The plasma concentration of the tracer is equal to the injected activity divided by the plasma volume, $C_{p,0} = A_{inj}/PV$.

$$C_p(t) = \frac{A_{inj}}{F_p \cdot E} \tag{26}$$

The clearance is the amount of tracer that is cleared from the blood plasma over time (equation 27).

$$Cl = A_{inj}/C_p(t) \tag{27}$$

A combination of equation 26 and 27 gives:

$$Cl = F_p \cdot E \tag{28}$$

Clearance is equal to the plasma flow multiplied by the excretion. Recall Frick's principle (equation 19) and the assumption about the mean concentration of the tracer in the plasma, and this will result in a tracer concentration in the vein that equals to zero. Combining Frick's principle with equation 28:

$$\frac{dA}{dt} = F_p(c_a \cdot c_v) \cdot E = F_p \cdot C_p \cdot E = Cl \cdot C_p \tag{29}$$

The relation given in 29 is valid under the assumptions mentioned earlier and is therefore only of use before the excretion of the tracer from the kidneys has begun. Integration of equation 29 gives:

$$\int \frac{dA_{org}}{dt} = Cl \cdot \int C_p(t)dt \Rightarrow A_{org} = Cl \int C_p(t)dt \tag{30}$$

Equation 30 can now be rewritten as a sum for the left and the right kidney:

$$A_{org} = A_{dx}(t) + A_{sin}(t) = Cl_{dx} \cdot \int C_p(t)dt + Cl_{sin} \cdot \int C_p(t)dt$$

$$= (Cl_{dx} + Cl_{sin}) \int C_p(t)dt \tag{31}$$

The function of the right kidney, as a function of the clearance gives the following expression:

$$\frac{Cl_{dx}}{Cl_{dx} + Cl_{sin}} = \frac{A(t)_{dx}}{A(t)_{dx} + A(t)_{sin}} \tag{32}$$

Where $A(t)_{dx}$ is the activity in the right kidney and $A(t)_{sin}$ is the activity in the left kidney. One can further assume that the count rate is proportional to the kidney activity assuming the proportionality constant is the same for the left and right kidney.

$$\frac{Cl_{dx}}{Cl_{dx} + Cl_{sin}} = \frac{R(t)_{dx}}{R(t)_{dx} + R(t)_{sin}} \tag{33}$$

where $R(t)_{dx}$ and $R(t)_{sin}$ is the background corrected count rate in the left and right kidney respectively. The relation derived above is only valid when the kidneys are positioned at the same depth. Assuming that the position is the same for both kidneys, then the perceptual split function can be calculated according to equation 34 and 35 for the right kidney function, RKF, and left kidney function, LKF:

$$RKF(\%) = \frac{R_{dx,p}(t)}{R_{dx,p}(t) + R_{sin,p}(t)} \cdot 100\% \tag{34}$$

$$LKF(\%) = \frac{R_{sin,p}(t)}{R_{dx,p}(t) + R_{sin,p}(t)} \cdot 100\% \tag{35}$$

$R_{sin,p}(t)$ and $R_{dx,p}(t)$ is the background corrected count rates for the posterior view. For calculation made with GM images, corrected countrates can be calculated according to equation 36 and 37.

$$RKF_{GM}(\%) = \frac{\sqrt{R_{dx,GM}(t) \cdot R_{dx,GM}}}{\sqrt{R_{dx,GM}(t) \cdot R_{dx,GM}} + \sqrt{R_{sin,GM}(t) \cdot R_{sin,GM}}} \cdot 100\% \tag{36}$$

$$LKF_{GM}(\%) = \frac{\sqrt{R_{sin,GM}(t) \cdot R_{sin,GM}}}{\sqrt{R_{sin,GM}(t) \cdot R_{sin,GM}} + \sqrt{R_{dx,GM}(t) \cdot R_{dx,GM}}} \cdot 100\% \tag{37}$$

This calculation of the split real function is based on the one given by Göran Graneus [1].

5 Materials and Methods

5.1 Monte Carlo Simulated Image Data

22 sets of phantom images were obtained from G Brolin et al. at Lund University Hospital. The split renal function ranged from 10% to 50% in steps of 5% for each image set. A so-called anthropomorphic cardiac-torso (XCAT) phantom is used in combination with the Monte Carlo (MC) code SIMIND [27, 28] to generate the simulated images. This combination is used to simulate very realistic dynamic renography images. Minor adjustments were made to obtain a more realistic and manageable radiopharmaceutical transport, for example a left and right ureter for illustration of tracer flow from the renal pelvis, also the heart blood pool was adjusted. A pharmacokinetic model was performed by G Brolin et al. to define a dynamic whole-body activity distribution. For detailed information about the anthropomorphic digital phantom and the adjustments made, the reader is referred to G Brolinet al. [29].

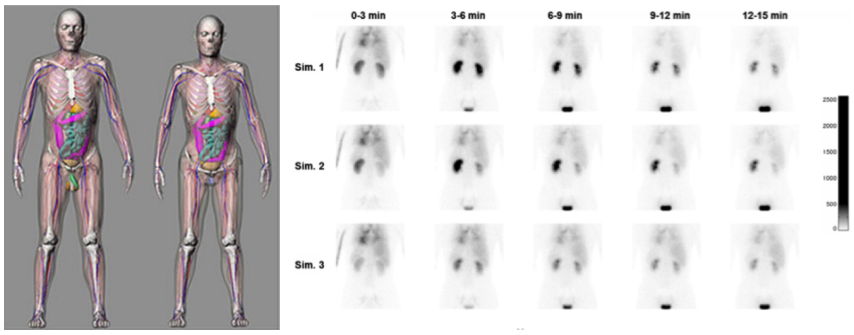

Figure 8: To the left an illustration of the cardiac-torso (XCAT) phantom [7], to the right the simulated XCAT renography images, the time is in minutes post injection [8].

The simulated images contain known values of the split renal function. When applying different background ROIs, a comparison between the split renal function obtained for different background ROIs and the known value can be made.

5.2 KYOTO KAGAKU Phantom Measurements

A set of measurements was performed with the abdomen kyoto KAGAKU phantom. The abdomen phantom consists of kidneys, liver and a part of the vertebral column enclosed in a fillable, elliptical cylinder, see figure 9.

Figure 9: Kyoto KAGAKU phantom filled with water.

5.2.1 Transmission Measurements

The phantom was filled with water and transmission measurements were performed with a ^{57}Co flood source placed on the lower detector. Images were acquired from the anterior view with the phantom on the gamma camera couch and one registration without the phantom (see figure 10). The purpose of this measurement was to enable attenuation correction according to 10. The chosen camera parameters can be seen in table 1. The obtained images were evaluated in IDL (interactive data language) to determine which measuring time yields the most suitable counting statistics for our measurements. This was done by placing a ROI in the image and extract the number of totally registered counts, the mean number of counts and number of pixels in the ROI. The ROIs can be seen in figure 10. In order to determine which measurement time was most suitable, line profiles where drawn in each of the acquired images.

Table 1: Camera parameters.

Collimator	LEGP
Matrix size	128x128
Pixel size	4,7 mm
Measurement time	5 min
Sensitivity	138 $s^{-1}MBq^{-1}$
Detector configuration	180^0
Energy window width	20%
Zoom factor	1.0
FOV	50,8 x 38,1 cm

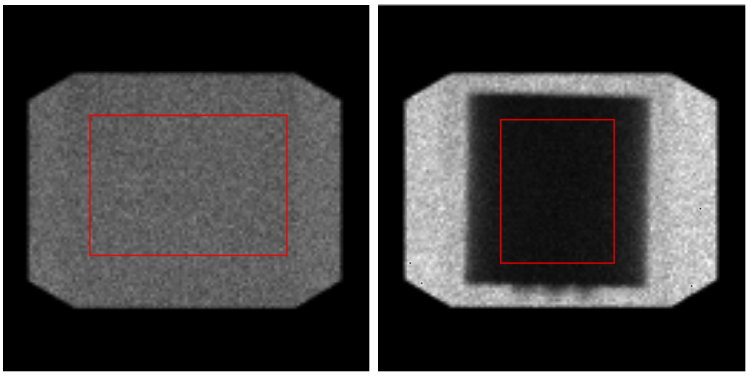

Figure 10: Left; ROI in the 'blank' image and right; the ROI in the image acquired with the phantom on the gamma camera couch.

5.2.2 Absolute Measurement of Activity

To determine how much activity should be added to the different parts of the phantom (kidneys, liver and background); the simulated images were used. The simulated image that corresponded to a split renal function of 50/50% was chosen. The simulated images were made to obtain images that correspond to good image quality and which simulates a real patient examination as much as possible. ROIs are drawn manually in each kidney and also in the liver and in the background. From each ROI, the counts per pixel were extracted. The total count rates were divided with the detector sensitivity,ϵ ([counts/s]/[s][MBq]) to determine organ activity. The pixel size was multiplied with the total amount of pixels in the ROIs and the organ thickness. To determine the organ thickness, the phantom was disassembled and the kidneys and liver was weighted with and without water (see table 2). The calculated activity is shown in table 2

Table 2: Phantom characteristics for measurements.

organ	weight (no water) [g]	wight (water) [g]	calculated activity [MBq]
kidney sin	104.84	277.61	17.80
kidney dx	106.83	281.79	16.70
liver	529.75	2299.5	10.60

The calculated activity was administered to the phantom followed by imaging. To enable depth correction by applying geometric mean, the measurement were performed using the conjugate view. The activity quantification was performed according to equation for Gate and Kojima background correction (equation 13, 14, 15 and 16).

The absolute activity was calculated using equation 9 where the rescaled attenuation coefficicent is used (equation 12). The activity concentration was calculated with different background correction methods. The methods used were Gates method (equation 13 and 14) and Kojima method (equation 15 and

16). These calculations are performed in IDL.

5.3 Region of Interest for Patient and Simulated Images

At Helsingborg's general hospital, dynamic images are recorded for 21 minutes; a total of 84 images are obtained (15 s/image). An aorta ROI is drawn in the images acquired during the first minute after injection because the aorta is more prominent in these images. The images acquired during the subsequent minutes show the kidneys ability to extract the tracer from the blood. To enable a good border detection of the kidneys, but at the same time avoiding inclusion of the renal pelvis in the kidney ROI, image 5-16 (1,15 - 240 s) were added to a total image and on these addition images, the kidney and background ROIs were drawn whereas aorta ROI is drawn on image 1-4 (15,00 -60,00 s). The background ROI is expressed as CPS/pixel multiplied with the number of pixels in the kidney ROI. The result is then subtracted from CPS within the kidney-ROI. The drawing of the ROIs are done both manually and automatically.

22 images were obtained from Lund University Hospital, but only 18 images where evaluated. The automated program encounters problems when distinguishing the kidney borders and is not reliable in the interval 1-9 %, though a split renal function of 0 and 10 % is reliable. This means that a kidney function of 0 % and 10 % is given from the program but the deviations are large for values between 1-9 %, a given value of 5 % can as well be 8 % and vice versa.

The automated ROI:s applied on all images are adjacent lateral background ROI, adjacent perirenal background ROI and distant background ROI (figure 11). The maximum allowed deviation for the automated ROI to the simulated images was set to 5%.

Figure 11: **Left:** Adjacent lateral ROI **Middle:** Adjacent perirenal ROI **Right:**Distant perirenal ROI.

- **Distant perirenal background ROI:** 2 pixels wide and 4 pixels outside the kidney ROI.
- **Adjacent perirenal background ROI:** 2 pixels wide and 1 pixel outside the kidney ROI.
- **Adjacent lateral background ROI:** 2 pixels wide and 1 pixel outside the kidney ROI but with a C-shaped stucture.

The evaluation technique is presented below:

1. The three automated methods were applied on the simulated images.
2. The lateral ROI method was applied manually on the simulated images by a physician at Helsingborg's general hospital.
3. The automated and manually drawn ROIs were compared to the "true" split renal function value from the simulated images. Maximum allowed deviation was 5 %; a limit given from the accountable physician.
4. The automated ROI method that gave values that best corresponded to the "true" split renal function was applied on the patient data.
5. Manual lateral ROI method was applied on all patients
6. 4 and 5 were performed with ROI drawing on posterior images and also on geometric mean corrected images.
7. 4 was additionally performed with attenuation-and geometric mean correction.

An example of the manually drawn lateral ROI is given in figure 12, and the automated distant perirenal ROI in figure 13.

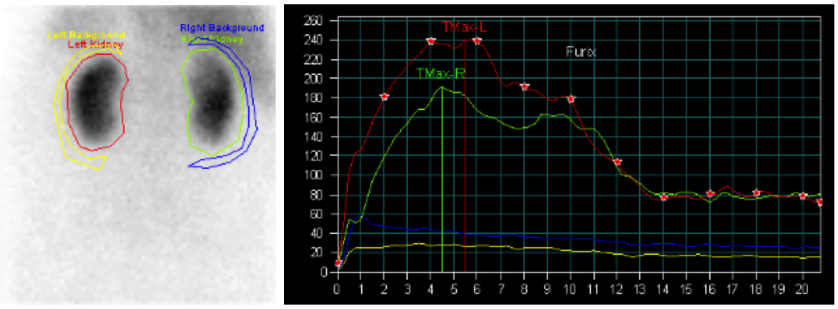

Figure 12: *Left:* The drawing of kidney and background ROI at Helsingborg hospital. *Right:* Diagram of the counts per second graphed over time.

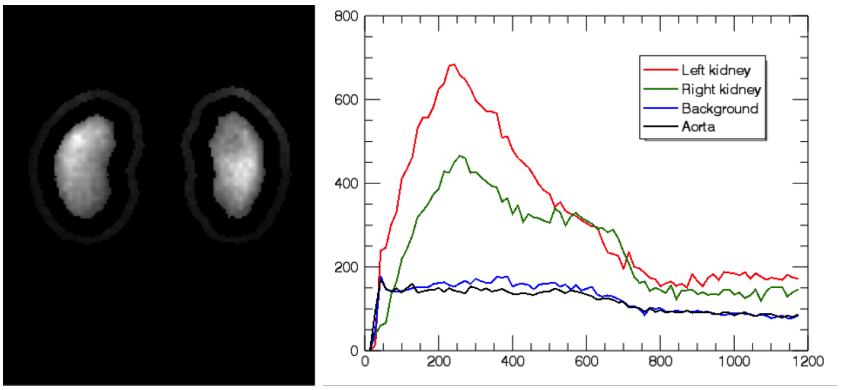

Figure 13: *Left:* The drawing of kidney and background ROI in the automated program. *Right:* Diagram of the counts per second graphed over time.

5.4 Assessment of Simulated Images

The 18 images were chosen for manual and automatic evaluation. The advantage with the simulated images is that they enable comparison of the different methods against a known split renal function value. Solely posterior view was obtained for the simulated images. For this reason, the geometric mean correction could not be applied on these images. The three different background ROI mentioned in the previous section (Region of Interest for Patient and Simulated Images) were applied on the posterior image with the automated program. The 22 images were also evaluated manually, where kidney and background ROIs were drawn solely with the adjacent lateral background method. The calculation of the split renal function for the different ROIs applied was done according to equation 10.1 for the automated ROI. The manual evaluation was performed on a Siemens dual headed gamma camera renal evaluation program. For the simulated images used, the total split renal function is always 100 %.

5.5 Assessment of Patient Images

25 randomly chosen patients seeking health care for different reasons and referred to the physiological department for a renography at the general hospital in Helsingborg, Sweden, where included in this study. The personnel performing the examination were instructed via written instructions. Before injecting the patient with the radiopharmaceutical, a 5 minute transmission measurement of the patient was recorded with a ^{57}Co flood source. A blank image was also recorded for 5 minutes, with no patient on the couch. The transmission image and the blank image were then divided in order to correct for attenuation in the patient (see figure 9), according to equation 10. The transmission image was divided with the blank image according to 10 and then multiplied with the conjugate view (anterior + posterior) image. Posterior patient images were evaluated without attenuation correction as is the current practice at the department.

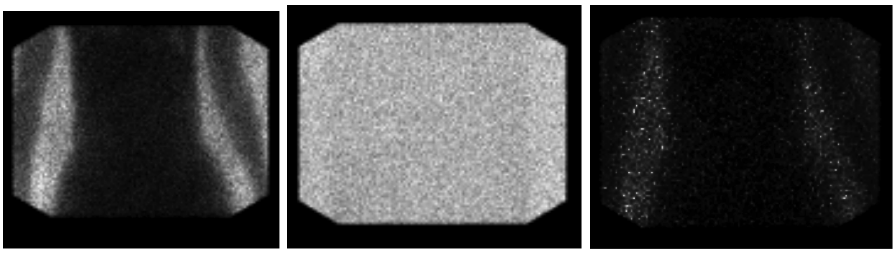

Figure 14: **Left:** Transmission image, **Middle:** Blank image **Right:** Divided image.

As mentioned before, the patient images were assessed with three different methods:

1. ROI drawing on the posterior image and Gates background correction with manual adjacent lateral background ROI and automated distant background ROI.

2. ROI drawing on the geometric mean images and Gates background correction with manual adjacent lateral background ROI and automated distant background ROI.

3. Transmission image multiplied with conjugate view followed of ROI drawing and Gates background correction.

The patient characteristics is shown in table 3.

Table 3: Patient age and sex.

Patient no	Age	Sex
1	28	F
2 *	64	M
3*	76	F
4^k	78	M
5^k	44	M
6	60	F
7	31	M
8	70	M
9*	33	F
$10^{k,*}$	80	M
11	70	M
12	37	M
13*	69	M
14*	16	F
15*	81	F
16*	75	F
17	74	M
18	80	M
19	62	M
20	30	M
21^k	83	M
22*	52	M
23*	70	M
24	73	F
25	71	F

The patients marked with k are patients with potential bilateral disease in which the split renal function can be misleading. In patients marked with * the kidneys are positioned at different depths which implicated need for depth correction via geometric mean correction or alternative methods. The depth difference is defined as the difference in kidney position relative to the contralateral kidney (see figure 15). For patient 4, 8, 9, 12 and 19, the physician used the geometric mean assessment when concluding the final statement.

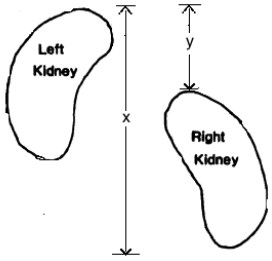

Figure 15: Definition of kidney depth, x/y.

6 Results

6.1 KYOTO KAGAKU Phantom Measurements

The physical phantom was used to:

1. Obtain optimal measurement time to determine attenuation in patient (6.1.1)
2. Perform activity quantification (6.1.2)

6.1.1 Transmission Measurement

As mentioned before the KYOTO KAGAKU phantom was filled with water and a ^{57}Co flood source was places on the lower detector. The total counts in each image (figure 10) for the three different measurement times can be seen in table 4.

Table 4: Results of the transmission measurements.

Time [min]	Counts phantom	Counts 'blank'	Difference
2	5 693	35 243	29 550
5	45 641	278 640	232 999
10	28 1108	438 519	157 411

In order to determine which measurement time was most suitable, line profiles were drawn in each of the acquired images. These can be seen in figure 16. The expected appearance of the line profile is a box shaped profile. Judging from figure 16, the 2 minute image is very noisy with few counts registered and can therefore be ruled out immediately. As for the remaining two images the profiles are similar, therefore the measurement time of 5 min was chosen for the patient studies since it is more convenient for the patients with as short an examination time as possible.

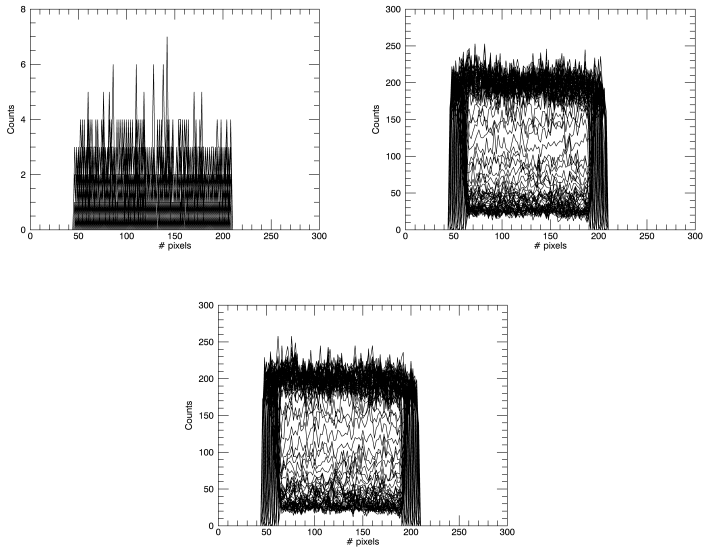

Figure 16: Line profiles through the transmisson images for a measurement time of 2 (top left image), 5 (top right image) and 10 min (bottom image).

6.1.2 Absolute Measurement of Activity

The images were registered with an anterior and a posterior detector simultaneously for 10 minutes. The equation used to calculate activity in figure 17 is shown in equation 9. Table 5 shows the absolute activity for both methods used to subtract background counts. The Gates method was calculated according to equation 13 and 14 and the Kojima method was performed according to equation 15 and 16. Both Gates and Kojima method are used in combination with equation 9, where the count rate R_A and R_B is corrected for according to Gates and Kojima.

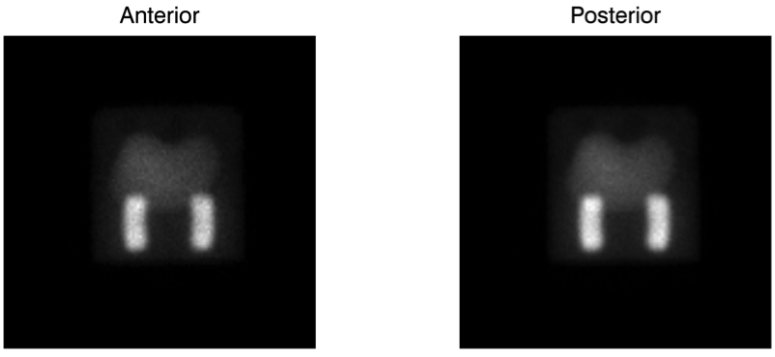

Figure 17: Anterior (left) and posterior (right) images of the KYOTO KAGAKU phantom filled with activity as shown in table 5.

Table 5: Resultant calculations of absolute activity.

Organ	Injected Activity [MBq]	Absolute activity Gates [MBq]	Absolute activity Kojima [MBq]
Left kidney	18,85	20,09	18,34
Right kidney	18,69	20,74	19,90

6.2 Simulated images

Table 6 shows the split kidney function for the left and the right kidney. Only the kidney function in the interval 50-10% were chosen for analysis. The simulated images were evaluated with the three different background ROIs. The distant perirenal background ROI, adjacent perirenal background ROI and the adjacent lateral background ROI (automatically and manually applied)(figure 11).

Table 6: Capital letter regards left and right kidney with the same degree of function reduction on simulated images.

Label left and right kidney	Split kidney (left-right)	function [%] (right-left)
A	50-(50)	50-(50)
B	45-(55)	45-(55)
C	40-(60)	40-(60)
D	35-(65)	35-(65)
E	30-(70)	30-(70)
F	25-(75)	25-(75)
G	20-(80)	20-(80)
H	15-(85)	15-(85)
I	10-(90)	10-(90)

The deviation from the real value of all assessments are shown in bar chart 1 and 2. Bar chart 1 shows the values for the left kidney and bar chart 2 the values for the right kidney. The dashed line in the bar chart shows the "maximum allowed deviation" from the real value which is set to 5%. The numerical values for bar chart 1 and 2 can be seen in Appendix II. Bar chart 1 and 2 show that the distant background ROI gives the smallest deviation from the true value for both the left and the right kidney and gives the best results especially for the right kidney. Therefore the distant background ROI is chosen to be applied to the patient images.

Bar chart 1: Deviation for relative left kidney function

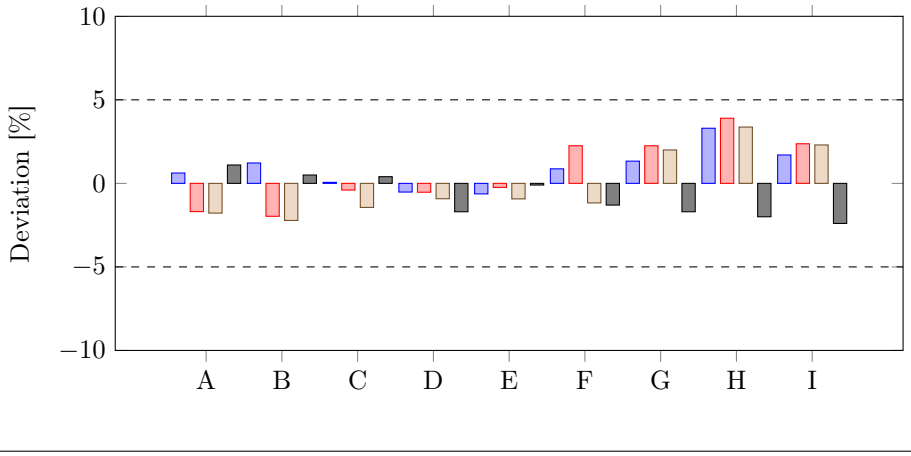

Bar chart 2: Deviation for relative right kidney function

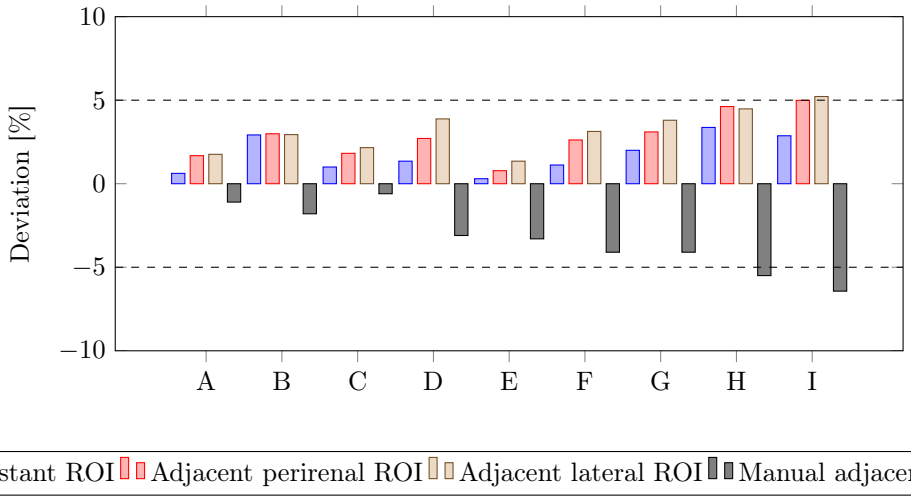

6.3 Patient Study

Table 7 show patient characteristics.

Table 7: Patient charaterstics.

Patient no	Charateristics
2	*
3	*
4	k
5	k
9	*
10	k
13	*
14	*
15	*
16	*
21	k
22	*
23	*

The patients marked with k are patients with potential bilateral disease, in which case the split renal function can be misleading. In patients marked with * the kidneys are positioned at different depths which implicated a need for depth correction via geometric mean calculation or other alternative methods. The depth difference is defined as the difference in kidney position relative to the contralateral kidney. For patient 4, 8, 9, 12 and 19, the physician used the geometric mean assessment when concluding the final statement.

6.3.1 Evaluation of Posterior Images

Bar chart 3 and 4 show the deviation of the relative kidney function for 25 patients. The value obtained with the automated distant ROI is chosen as the reference and put as 0 on the y-axis. The deviation in manual assessment (expressed in percentage points) is shown on the y-axis in both figures. The numerical values corresponding to bar chart 3 and 4 are given in Appendix III.

Barchart 3: Deviation expressed in percentagel points in left kidney

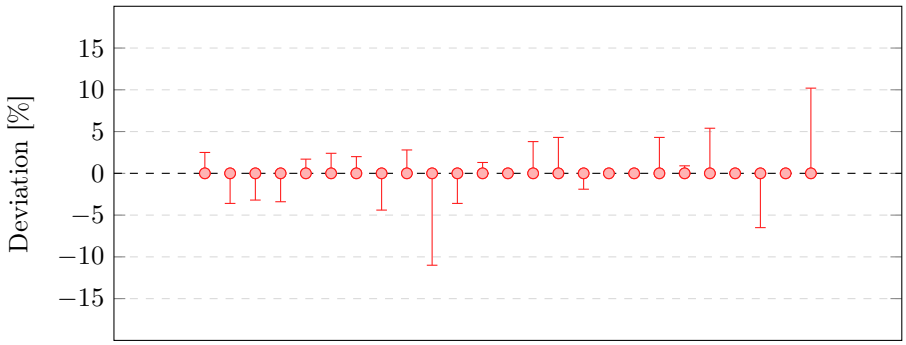

Bar chart 4: Deviation expressed in percentage points in right kidney

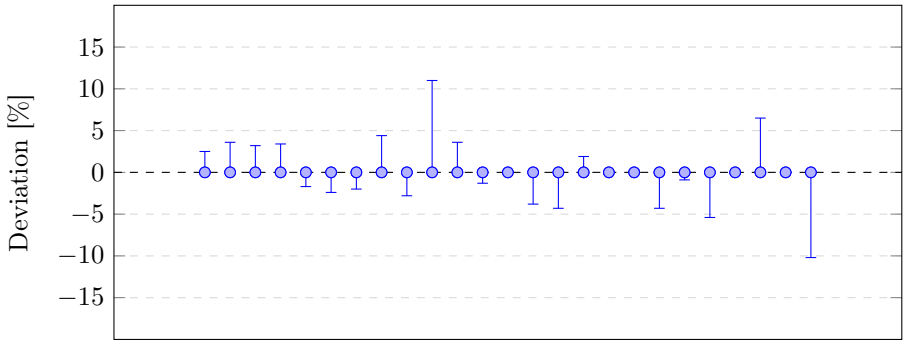

6.3.2 Evaluation of Anterior and Posterior Images

Bar chart 5 and 6 show the deviation of the relative kidney function for 25 patient studies. The value obtained with the automated distant ROI for geometric mean correction and attenuation correction is chosen as the reference and put as 0 on the y-axis. The deviation in manual assessment for geometric mean (expressed in percentage points) is shown on the y-axis in both figures. The numerical values corresponding to bar chart 5 and 6 are given in Appendix III.

Bar chart 5: Deviation expressen in percentage points in left kidney.

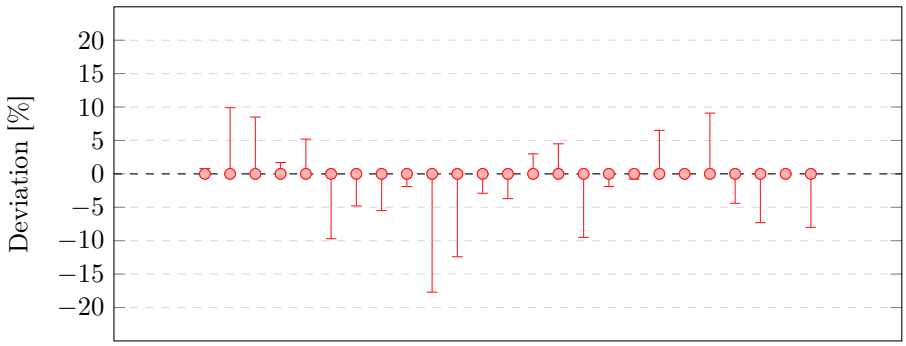

Bar chart 6: Deviation expressed in percentage points in right kidney.

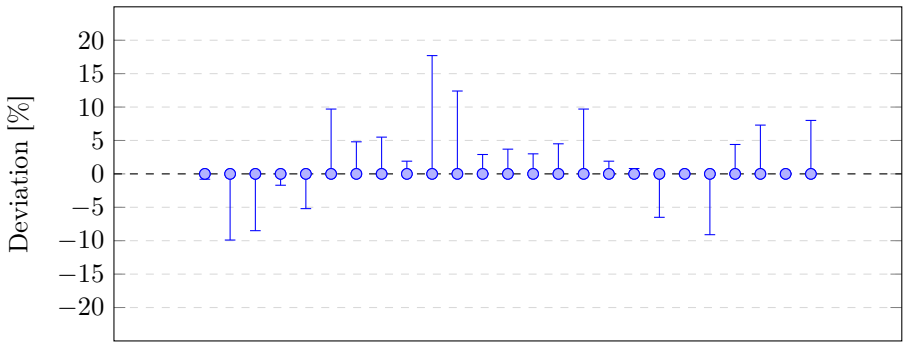

6.3.3 Evaluation with Attenuation Correction

To analyze the importance of attenuation correction, the geometric mean with automated distant ROI background correction was applied in combination with attenuation correction (equation 11) and is set to zero in bar chart 7. These results are then compared to the one obtained with the geometric mean with distant automated background correction. The deviation between the split renal function value of the left kidney is shown in bar chart 7.

Bar chart 7: Deviation expressed in percentage points in left kidney.

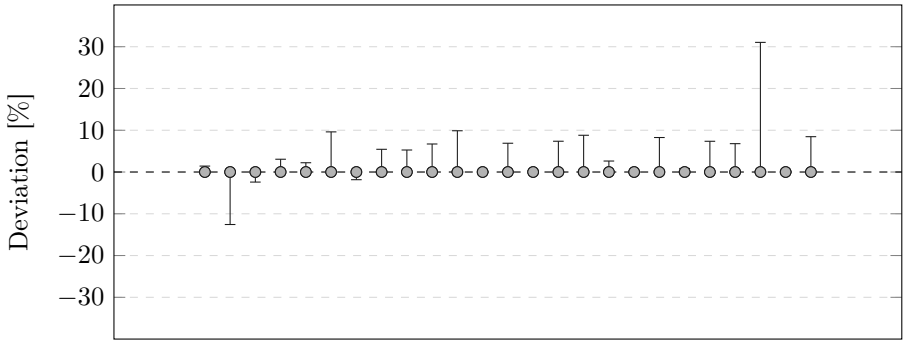

Bar chart 8: Deviation expressed in percentage points for geometric mean title

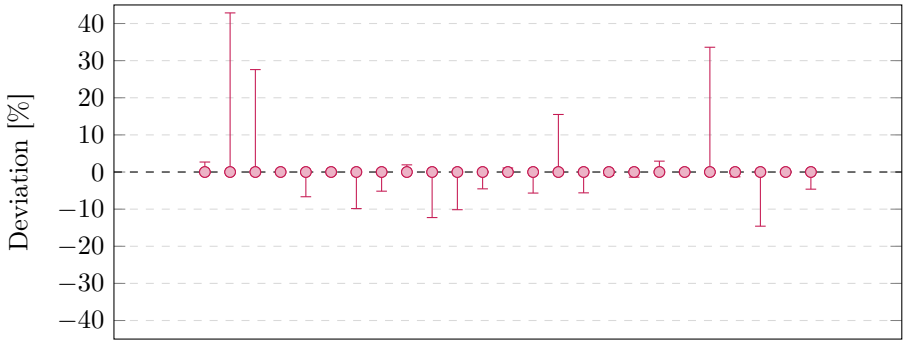

;

7 Discussion

This work is divided into several parts which sums up in concluding which factors affect the split renal function of the kidneys. Initially, phantom measurements on a Kyoto Kagaku phantom were made. These measurements had dual purposes. Activity quantification and determining time for transmission measurements. The activity quantification included calculations with the Gates and the Kojima method, where the Kojima method yielded the most accurate results. This was as expected, but the calculations require the operator to know the kidney depth. If the Kojima method is to be performed in the clinical context, an image acquiring data from the patients side view is needed, so the estimation of the kidney depth can be enabled. The transmission measurements are used to correct for attenuation in the patient.

The use of 21 simulated images enabled estimation of errors associated with different application of background ROIs (automatic distant perirenal ROI, automatic adjacent perirenal ROI, automatic adjacent lateral ROI and manual adjacent lateral ROI). Since the choice of background correction is debated, the need for a thorough investigation of the different methods are essential to find the most suitable background correction method. The results show that the distant background ROI gives the smallest error, which means that this background correction method is the most suitable out of the three possible. Choosing a ROI which is slightly more separated from the kidney minimizes inclusion of renal activity in the background ROI according to A Taylor et al [5]. This statement is verified by the performed measurements for the distant background correction method as well. This could be a result of the partial volume effect which means that the signal smears out into adjacent pixels and if these counts are registered in the background ROI, the background will be overestimated, and thus could lead to an underestimation of the kidney uptake. Since the distant ROI method gave values that best correspond to that of the true kidney function, this ROI method was chosen to be applied on the patient images. In the consensus report composed by A. Prigent et al, it is argued in favor of the perirenal ROIs, preferably one or two pixels from the kidney ROI. Perirenal rectangular or circular background ROI without a specified distance between the kidney and the background ROI is also the recommendations given in the EANM pediatric guidelines [16,15]. A. Taylor et al conclude that automatic perirenal and elliptical ROIs are more reproducible then the lateral ROI. They also state that the use of automated ROIs will minimize interobserver and intraobserver variability [5]. Automated ROI is not standard at all clinics and manually drawing perirenal ROIs will be time consuming and therefore not applicable in clinical context. Therefore, clinics that draw kidney and background ROI automatically chose the lateral ROI.

The use of the geometric mean method is well known to be a highly accurate technique in nuclear medicine, and the influence of kidney depth variations in renography has long been understood. The use of conjugate view is of great importance for asymmetric kidneys e.g. ectopic kidneys. It has not been recommended in pediatric care but plays an essential role in standard procedures for adults [15]. A. F. Yapar et al. concluded in their study that the geometric mean correction method in split renal function calculations differ significantly from the use of posterior view [31]. One can also argue that the conjugate view registrations fixates the patient more, which decreases the possibility of inducing motion artifacts since an anterior detector close to the patient prevent movement to some extent. When only posterior view is used, the space over the patient is free and the tendency to move is presumably more substantial. There is a concern with the conjugate view if the patient need to urinate during the exam, pausing the exam for the patient and then resume quickly, could be perceived as problematic for the personnel. Since only information obtained during the first 2-4 minutes of the exam is used to calculate the split renal function, the continuing exam can be carried out with only the posterior view detector if pausing is needed. It is also of great importance to understand the clinical context and that the theoretically best metods is not always the most suitable in the clinic. Two detectors placed close to the patient body can induce a claustrophobic feeling for the patient. Therefore a good communication and

understanding lay the basis for best health care. Nevertheless the stated results and existing studies argue for the advantage of the use of the geometric mean method. The geometric mean should be considered in all patients but especially when anatomical abnormalities are suspected.

Evaluation of the patient images is more complex since the real function is not known. Here the deviation between the two evaluation forms, automatic distant perirenal ROI and manual adjacent lateral ROI, are studied. Supposing the distant perirenal ROI gives a more accurate value, based on the conclusions made with the results from the simulated images, we suppose the same conclusion is stated for the patient images. Therefore the automatic ROI program is used as a golden standard in this study. Statistically the small sample size gives a vague statistical significance. It would therefore be of interest to carry out a study over a larger cohort of patients and examine if this conclusion is significant. We can however, conclude that the geometric mean correction is giving us values that is more correct than if not used.

Errors associated with the kidney depth can be corrected as mentioned if geometric mean correction is performed. But also via performing a CT (computed tomography) scan. From a realistic point of view, the CT scan is inappropriate to perform for each patient. The absorbed dose from a CT scan are relatively high compared to other imaging modalities. Even if prior CT-examinations of patients have been carried out, these cannot be used since contrast used in CT is believed to cause transient swelling of the kidneys which implicates underestimation of the true kidney-to-skin distance. Another possibility is a lateral scan performed at the end of the dynamic acquisition or an ultrasonograpy [16]. A CT scan gives a degree of precision not possible with a scintigraphic lateral scan [32]. An issue with sonography is that the examination is performed in sitting position and the scintigraphy in a supine position, which can affect the position of the kidneys since they are not fixed in the abdomen. The geometric mean seems to be the most appropriate method for those clinics that have a dual-head gamma camera. There are pitfalls with the geometric mean method as well in clinical context. A difference in superposition of bones and bowel gas can occur and the background activity in renal ROIs can be affected by self-attenuation of kidneys with different sizes [16].

For patient 2, 3, 4, 10, 11, 13, 14 and 23, the deviation in the split renal function is quite large, in bar chart 4 and 5. Patient 10 and 23 have a degraded left and right kidney and this is also believed to be the case for patient 11, but not as severe as for the other two. The count rates in these kidneys is therefore low and the edge detection becomes more difficult, which can result in values of the split function that can be misleading since the total sum is always 100%. For patient 2, one kidney is twice the size of the other, and an explanation for the higher deviation could possibly be self-attenuation in the kidneys.

For the automated ROI drawing program compared to manually drawn ROIs there is a huge advantage when using automated ROIs. Especially when considering the operator dependence. It is difficult for different technologists, and in some cases physicans, to perform the assessment in exactly the same way and therefore manually drawn ROI induce an inter-operator variability. The

automated program would avoid this. But for poorly functional kidneys there is a concern. The border detection will become problematic. For patients where both kidneys have a severely reduced function, the program will have a problem of identifying borders. This also raises another question; that if renography is suitable for patients in which the function in both kidneys is severely reduced. In those cases, the contribution depends on the clinical question or problem. There lies an interest in discussing the pros and cons of the automated ROI program in comparison to manually drawn ROI in its clinical context. The work burden on the personnel would decrease if the assessment was automated. A totally automated program could however pose a problem if the personnel relies entirely on the program. By placing a box over each kidney and then observing the final kidney and background ROI mask, the personnel can participate in the process and if a problem emerges, it will be more likely that they will observe it. A combination of manual and automated ROIs is also an alternative. If the personnel should feel that the program is performing an incorrect ROI extraction, they can perform the drawing manually. And finally an alternative to manually drawn kidney ROIs and automated background ROIs would be of interest, since different renal ROIs perform equally well for split renal function as long as the renal function is not severely degraded. This does however pose a problem in terms of reproducibility and accuracy when determining the relative renal function [16]. Such a program has been created but has not been applied in the scope of this study. In addition to the changes listed above, the performance of a separate program only applied on poorly functional kidneys would be interesting to study. This could be done by creating a program which sums additional images. Usually only image 5-16 is used to avoid including the extraction phase in the renal ROI. For poorly functional kidneys the uptake phase is longer and inclusion of other images could be a solution.

Attenuation can for some patients have an effect on the total split renal function. This effect increases for overweight patients and for patient where the kidney size varies. But performing transmission measurements on all patients can be time consuming for the personnel and is not a reasonable solution to this problem.

Limitations of the study lie in the fact that the patient sample size is small and therefore no statistical test have been applied. Also, the automated ROI program has room for improvements towards totally automated or partially automated drawing of ROIs. Another interesting point of view is studying simulated images where the conjugate view is applied. This would enable verification of the geometric mean and give an exact percent of the deviation from posterior view evaluations. It is also important to mention that phantoms, and especially physical phantoms, has a difficulty in precisely imitate actual patients for instance the bowel and patient movement. But it is ideal when verifying a reliable assessment on image modalities.

8 Conclusion

Our results support the application of a distant ROI method when calculating the split renal function preferably applied with an automated ROI program

to avoid inter-operator variability. The geometric mean method can probably be recommended as a standard method in clinics. For patients with severely reduced kidney function, the calculated split function can be unreliable. Focus lies on understanding the physiology and pathophysiology of the kidneys and the limitations and pitfalls of planar imaging with gamma cameras.

9 References

1. Göran Granerus (2000). *Njurarna och övre urinvägarna metod använd inom klinisk fysiologi för diagnostik och funktionsvärdering.* Sweden: Studentlitteratur, Lund, 1-261.

2. Lena Johansson. (2011). *Renografi, Presentation av enkät.* Available: www. equalis.se./media/47340/lena%20johansson_1.pdf Last accessed 26th Feb 2014.

3. A Boubaker, J.O. Prior, J-Y Meuwly et al. (2006). Radionuclide Investigation of the Urinary Tract in Era of Mulrimodality Imaging. *J Nucl Med.* 47 (11), 1819-1836.

4. Amy Piepsz, Marianne Tondeur and Hamphrey Ham. (1999). Relative ^{99m}Tc-MAGR$_3$ renal Uptake: Reproducibility andAccuracy. *J Nucl Med.* 40 (1), 972-976.

5. A Taylor, Jr, K Thakore, R Folks et al . (1997). Background Subtraction in Technetium-99m-MAG3 Renography. *J Nucl Med.* 38 (1), 74-79.

6. A Eskild-Jensen, I Gordon et al. (2004). Interpretation of the renogram: problems and pitfalls in hydronephrosis in children. *BJU International.* 94 (1), 887-892.

7. A. G. Graha, J. S. Scott, I Kennedy et al. (1967). Clinical experience with renal scanning using Hg 197 clormerodin. *British journal of urology* . 718-726.

8. J.S. Fleming. (1979). A Technique for the Absolute Measurement of Activity Using a Gamma Camera and Computer. *Physics in Medical and Biology-IOPScience.* 24 (1), 176-180.

9. King M, Farncombe T. (2003). An Overwiew of Attenuation and Scatter Correction of Planar and SPECT Data of Dosimetry Studies. *Cancer biotherapy radiopharmaceuticals.* 18 (2), 181-190.

10. David Minark, Katarina Sjögren and Michael Ljungberg. (2005). A New Method to Obtain Transmission Images for Planar Whole-Body Acitivity Quantification. *Cancer biotherapy radiopharmaceuticals.* 20 (1), 72-76.

11. Y Takaki, A Kojima, A Tsuji et al. (1993). Auantification fo Renal Uptake of Technetium-99m-DTPA Using Planar Scintigraphy: A Technique That Considers Organ Volume. *The Journal of Nuclear Medicine.* 34 (3), 1184-1189.

12. Gray F. Gates. (1982). Glomerular Filtration Rate: Estimation from Fractional Renal Accumulations of 99mTc-DTPA (Stannous). *American Roentgen Ray Society.* 128 (1), 565-570.

13. W C.A.M. Buijs, J A. Siegel, O S. Boerman and F H.M. Corstens. (1998). Absolute Organ Activity Estimated by Five Different Methods of Background Correction. *J Nucl Med.* 39 (1), 2167-2172.

14. Taylor A Jr, Thakore K, Folks E et al. (1997). Background subtraction in technetium-99m-MAG3 renography. *J Nucl Med.* 1 (1), 74-79.

15. Gordon I, Colarinha P, Fettich J, et al. Guidelines for standard and diuretic renography in children. *Eur J Nucl Med.* 2001;28: 21-30.

16. l. Prigent, P. Cosgriff, G. F. Gates et al. (1999). Consensus report on quality control of quantitative measurements of renal function obtained from the renogram: International consensus committee from the scientific committee of radionuclides in nephrourology. *Seminars in Nuclear Medicine.* 29 (2), 146-159.

17. Miriam A. Wallace, RN1. (1998). Anatomy and Physiology of the Kidney. *AORN Journal.* 68 (5), 799-820.

18. Bertil Sonesson and Gun Sonesson (2008). *Anatomi och fysiologi.* 4th ed. Korotan, Ljubljana, Slovenia: Repro 8 AB, Nacka. 9-396.

19. Lori Candela and Carolyn Yucha. (2004). Renal Regulation of Extracellular Fluid Volume and Osmolality. *Nephrology Nursing Journal.* 31 (4), 397-444.

20. Miles N. Wernick and John N. Aarsvold (2004). *Emission Tomography: The Fundamentals od PET and SPECT.* London, UK: Elsevier Academic Press. 1-576.

21. Magdy. M Khalil (2011). *Basic Science of Nuclear Medicine.* Berlin Heidelberg: Springer-Verlag. 1-423.

22. Bubeck B, Brandau W, Weber E, et al. (1990). Pharmacokinetics of technetium-99m-MAG3 in humans. *J Nucl Med.* 31(1), 1285-1293.

23. Andrew Taylor. (1999). Radionuclides Renography: A Personal Approach. *Seminars in Nuclear Medicine.* XXIX (2), 102-127.

24. P.H. O'Reilly. (2002). Standardization of the renogram technique for investigating the dilated upper urinary tract and assessing the results of surgery. *BJU International.* 91 (1), 239-243.

25. A Piepsz, M Tondeur and H Ham. (1999). Relative ^{99m}Tc-MAG$_3$ Renal Uptake: Reproducibility and Accuracy. *The Journal of Nuclear Medicine.* 40 (6), 972-976.

26. Peter F. Sharp,Howard G. Gemmell and Alison D. Murray (2005). *Practical Nuclear Medicine.* 3rd ed. Singapore: Springer-Verlag. 205-229.

27. M. Ljungberg and S. E. Strand. (1989). A Monte Carlo Program from the simulation of scintillation camera characteristics . *Comput. Methods Programs Biomed.* 29, 257-272.

28. W P Segars, Sturgeon G,S Mendonca et al.. (2010). 4D XCAT phantom for multimodality imaging research . *Med. Phys.* 97 (1), 4909-4915.

29. Gustav Brolin, Katarina Sjögren Gleisner and Michael Ljungberg. (2013). Dynamic 99mTc-MAG3 renography: images for quality control obtained by combining pharmakochinetic modeling, a anthropomorphic computer phantom and Monte Carlo simulated scintillation camera images. *Phys. Med. Biol.* 58 (1), 3145-3161.

30. Ernest V. Garcis, Russell Folks et al. (2010). Definintion of Renal Region-of-interest for Tc-99m MAG3 Renograms: Validation in Patients with Normal Kidneys and in Patients with Suspected Renal Obstruction. *Nucl Med Commun.* 5 (31), 366-374.

31. A. F. Yapar, A. Mehmet, R. Mehemt et al. (2005). The conditions for which the geometric mean method revealed a more accurate calculation of relative renal function in ^{99m}Tc-DMSA scintigraphy. *Nuclar Medicin Communications.* 26 (2), 141-146. [Abstract avaliable]

32. Daniel C. Maneval, H. Lynn Magill et al. (1990). Measurement of Skin-to-Kidney Distance in Children: Implications for Quantitative Renography. *J NucIMed.* 1 (31), 287-291.

Figures

References

[1] J. S. Flemming, (1978), *Absolute Activity Measurement of Gamma Camera [ONLINE].*Available at: *http* : *//iopscience.iop.org*/0031 − 9155/24/1/017/*pdf*/0031 − $9155_2 4_{10}$17.*pdf*[Accessed 24 August 15].

[2] Henry Gray, (1981), *Anatomy of the Human Body Figure 1120 [ONLINE].* Available at: <*http* : *//www.bartleby.com*/107/*illus*1120.*html*> [Accessed 09 April 15].

[3] Henry Gray, (1981), *Anatomy of the Human Body Figure 1127 [ONLINE].* Available at: <*http* : *//www.bartleby.com*/107/*illus*1120.*html*> [Accessed 09 April 15].

[4] Henry Gray, (1981), *Anatomy of the Human Body Figure 1128 [ONLINE].* Available at: <*http* : *//www.bartleby.com*/107/*illus*1120.*html*> [Accessed 09 April 15].

[5] Henry Gray, (1981), *Anatomy of the Human Body Figure 1129 [ONLINE].* Available at:
<*http* : *www.bartleby.com*/107/*illus*1120.*html*> [Accessed 09 April 15]

[6] Björn Jonsson, Håkan Westling et.al. *Klinisk fysiologi* (1998). Stockholm: Liber AB p.320

[7] W. Paul Segars, (2015), $Segars_3 434[ONLINE].Availableat$:<*https://olv.duke.edu/xcat*> [*Accessed*03*September*15].

[8] Gustav Brolin, Katarina Sjögren Gleisner and Michael Ljungberg. *Dynamic 99mTc-MAG3 renography: images for quality control obtained by combining pharmakochinetic modeling, a anthropomorphic computer phantom and Monte Carlo simulated scintillation camera images* (2013). Phys. Med. Biol. 58 (1), 3145-3161.

10 Appendix I

10.1 Automated Region of Interest

This Appendix gives a step by step explanation of how the automated ROI program was constructed. Initially a box was placed around each kidney, see figure 18. Image 5-16 are then summed and squared to obtain a sharp edge. Image 5-16 is used at Helsingobrgs general hospital and it is believed to give the best kidney contour and avoid including the renal pevis in the the mask.

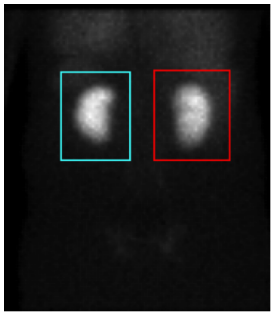

Figure 18: Position of box over each kidney.

Inside each box the values where set to 1 and outside to 0. Now the data inside each box can be processed. To enchance the contrast in the remaining box image, the function *hist_ equal* is used. A histogram is a graphic representation of numerical data and gives a density distribution. Further the data is integrated and a cumulative density probability function is obtained. An image threshold is applied, which generates a threshold value and is a simple form of image segmentation. With the help of a where function, the values below the threshold can be set to zero. How this *image_ threshold* is performed can be seen in the in the code-text below:

```
threshold=image_threshold(Bild,Threshold=t,/BYIMAGE,/MOMENTS)
Bild=where([threshold eq 0])=0
```

The histogram equalization and the image threshold function applied on the kidney box is shown in image 19.

By labeling the region in the image, the kidney contour and inner values are set as a region. With this function the program searches for objects and labels inside of the region. The region that is labelled here is the kidney where the pixel values in the kidney region is set to 1, label region applied on the kidney box is also shown in figure 19.

Now morphological operators can be applied on the image. To be specific, the "erode and dilate" function is used. Simply speaking, these operators are each others opposites. The dilate operator enlarges the boundaries of the pixels in the front portion. So the object 'grows' in size while holes within the object becomes smaller to a point at which they are totally filled. The erode operator

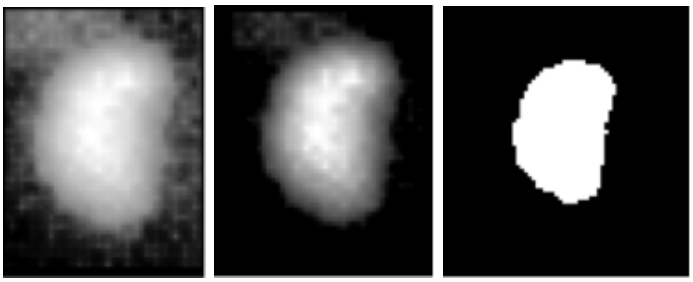

Figure 19: To the left: hist equal applied on the image and in the middle: image threshold. TO the right:

implementation 'shrink' or 'reduces' the object. For each of these functions, a structural element is defined. The structural element is a binary image or mask. It is typically smaller than the image that is being processed. When the morphological operator has been carried out, the structural element is translated to each pixel point in the image. The code for these operators used in the automated program is;

```
;;;;;;;;;;;;;;;;;;;;;;;;;;;;;;;;;;DILATE;;;;;;;;;;;;;;;;;;;;;;;;;;;;;;;;;;;;;;;;;;;;

radius = 10
strucElem = SHIFT(DIST(2*radius+1),radius, radius) LE radius

dilateimg=dilate(LABELS,strucElem)

;;;;;;;;;;;;;;;;;;;;;;;;;;;;;;;;;;ERODE;;;;;;;;;;;;;;;;;;;;;;;;;;;;;;;;;;;;;;;;;;;;;

radius_va = 10
strucElem_va = SHIFT(DIST(2*radius_va+1),radius_va, radius_va) LE radius_va

erodeimg_va= ERODE(dilateimg, strucElem_va, /GRAY)

;;;;;;;;;;;;;;;;;;;;;;;;;;;;;;;;;;;;;;;;;;;;;;;;;;;;;;;;;;;;;;;;;;;;;;;;;;;;;;;;;;;;;;;
```

The "erode and dilate" operator is applied on each mask that has been processed with the label "region". The objective is to be able to create a mask for degraded kidneys by enlarging the structures and filling the holes within the mask which can emerge for poorly functional kidneys. The mask is then 'shrunk' back to its normal size by applying the erosion operator. When this is done the mask is applied on all 84 images and the total count in the kidneys for each frame are registered.

As for the background, the "dilation" operator with different structural elements is used, one larger than the other and by subtracting these the background ROI is extracted. By varying the radius of the structural element, the ROI can be placed at different positions around the kidney ROI. The C-shaped background ROI is defined with the help of a for-loop, by setting a part of the pixels in the mask to zero:

```
;::::::::::::::::C-SHAPED BACKGROUND ROI::::::::::::::::::

for k=40,256 do begin
  diffdilateIm[k,*]=0
endfor

;::::::::::::::::::::::::::::::::::::::::::::::::::::::::::::
```

And finally an aorta ROI is defined. Here, a box ROI can be applied and placed over the pixels with the highest values, over the heart or aorta. In all the images used in this study, the aorta ROI is placed on descending aorta. By applying equation on the count-rate corrected for aorta and background the split left and right kidney function is calculated.

11 Appendix II

11.1 Numerical Values for Simulated Images

Table 8 and 9 shows the numerical data for bar chart 1 and 2 and also the real renal function.

Table 8: Deviation from renal function for right kidney for the simulated images

patient no	real value	Automated distal ROI	Automated perirenal ROI	Automated lateral ROI	Hbg-hospital[%]
1	50	0.62	-1.69	-1.78	1.1
2	45	1.22	-1.97	-2.22	0.5
3	40	0.06	-0.4	-1.44	0.4
4	35	-0.5	-0.53	-0.92	-1.7
5	30	0.63	-0.24	-0.93	-0.1
6	25	0.87	2.25	-1.17	-1,3
7	20	1.33	2.25	2	-1.7
8	25	3.3	3.9	3.37	-2.0
9	10	1.7	2.37	2.3	-2.4

Table 9: Deviation from renal function for right kidney for the simulated images

patient no	real value	Automated distal ROI	Automated perirenal ROI	Automated lateral ROI	Hbg-hospital[%]
1	50	0.62	1.68	1.76	-1.1
2	45	2.92	2.99	2.94	-1.8
3	40	1	1.82	2.16	-0.6
4	35	1.35	2.71	3.88	-3.1
5	30	0.3	0.78	1.35	-3.3
6	25	1.12	2.62	3.13	-4.1
7	20	2	3.10	3.80	-4.1
8	25	3.37	4.62	4.48	-5.5
9	10	2.87	4.99	5.22	-6.43

12 Appendix III

Numerical Values for Patient Study

Table 10: Relativ renal function for left kidney for the patient study

patient no	Auto ROI post	Manual post	Auto ROI GM	Manual GM	Auto ROI GM and transmission
1	63.7	66.2	64.2	65.0	63.3
2	20.1	23.7	15.3	25.0	17.5
3	46.3	43.1	28.3	37.0	29.0
4	64.1	62.2	63.9	62.2	62.0
5	53.4	55.1	59.9	54.7	58.6
6	33.2	35.6	47.9	43.4	43.7
7	54.8	55.0	58.8	54.0	59.9
8	78.2	77.6	75.6	68.0	71.7
9	54.0	56.8	59.9	58.0	56.9
10	62.0	49.0	65.2	53.6	61.1
11	60.8	56.9	80.1	65.5	72.9
12	51.9	53.2	59.8	56.9	59.6
13	74.1		68.3	64.6	63.9
14	55.4	51.6	53.1	49.9	52.9
15	68.5	72.8	59.7	64.2	55.6
16	69.9	68.0	71.7	62.2	65.9
17	53.8	53.6	54.6	52.7	53.2
18	57.6	57.3	57.9	57.1	57.9
19	53.1	57.4	53.3	59.8	58.1
20	58.3	58.2	59.5	59.4	59.0
21	89.9	95.2	77.3	96.2	72.0
22	50.3	49.9	58.2	53.8	54.5
23	79.8	63.9	91.6	59.7	69.9
24	100.0	100.0	100.0	100.0	100.0
25	53.7	63.9	70.0	62.0	65.0

Table 11: Relativ renal function for right kidney for the patient study

patient no	Auto ROI post	Manual post	Auto ROI GM	Manual GM	Auto ROI GM and transmission
1	36.3	33.8	35.8	36.6	36.7
2	79.7	76.3	84.7	74.8	82.5
3	53.7	56.9	71.7	74.8	71.0
4	35.9	39.3	36.1	37.8	38.0
5	46.6	44.9	40.1	45.3	41.4
6	66.8	64.4	52.1	56.2	56.3
7	45.2	45.0	41.2	46.0	40.1
8	24.6	22.4	24.4	32.0	28.3
9	46.0	43.2	40.1	42.0	43.1
10	38.0	49.0	34.8	46.4	38.4
11	39.2	43.1	19.9	34.5	27.9
12	48.1	46.8	40.2	43.1	40.4
13	25.9	37.0	31.7	35.4	36.1
14	44.6	48.4	46.9	50.1	47.1
15	31.5	27.2	40.2	35.8	44.4
16	30.1	32.0	28.3	37.8	34.1
17	46.2	46.4	45.4	47.3	46.8
18	42.4	42.7	42.1	42.9	42.1
19	46.9	42.6	46.7	40.2	41.9
20	41.7	40.8	40.5	40.6	41.0
21	10.2	4.8	22.7	3.82	28.8
22	49.7	49.9	41.8	46.2	45.5
23	20.2	36.1	8.42	40.3	30.1
24	0	0	0	0	0
25	46.3	36.1	30.0	38.0	35.0

13 Appendix

13.1 Possible Explanation to Deviatied Relative Kidney Function

Patient 3

Patient 3 showed deviation for geometric mean. The left kidney is positioned higher up relative the right kidney and sidelong in the abdomen.

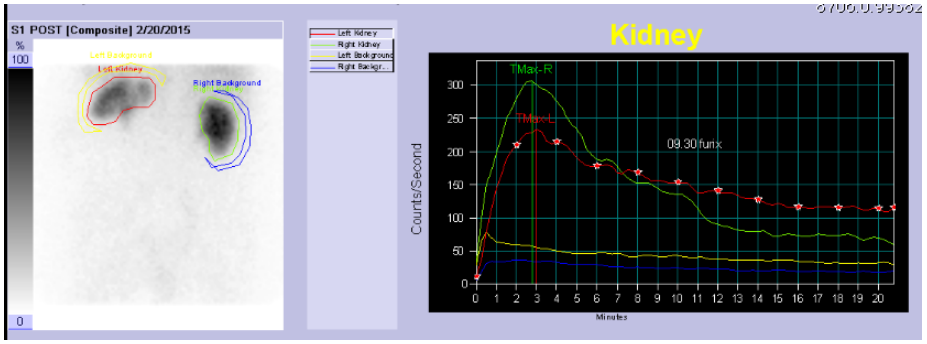

Patient 10

The kidneys function is severally reduced, slightly more reduced uptake bilateral. The creatinine registered 6 months before the renography was performed was 164 μmol/L (normale creatinine is 105 μmol/L). The deviations in the relative kidney function for this patient could be due to the fact that the total kidney function is reduced.

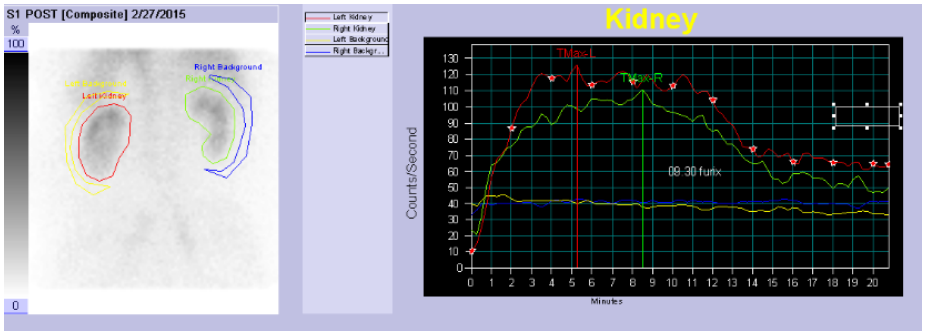

Patient 13

1. The right kidney has high-proof excretion obstruction and on the TAC a rapidly raising excretion phase can be observed.

2. It is also a possibility that the left kidneys background ROI is placed to close to the kidney ROI which lead to a underestimation of the left kidneys and consequently a overestimation of the right kidney function. When redrawing the kidney and background lateral ROI manually the relative kidney function was 70-30%.

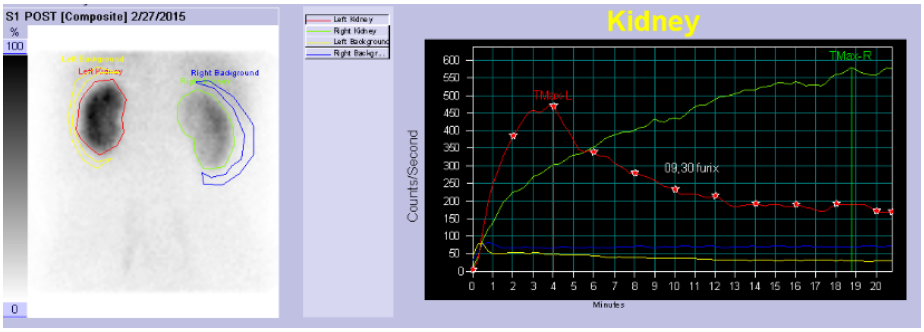

Patient 15

The kidneys have different size relative each other. The patient has been diagnosed with a right-sided kidney tumor with a reduced uptake caudal/medial in the right kidney. The background manual lateral ROI is drawn to close to the kidney ROI. New manual lateral evaluation gave a relative kidney function of 68-32 %.

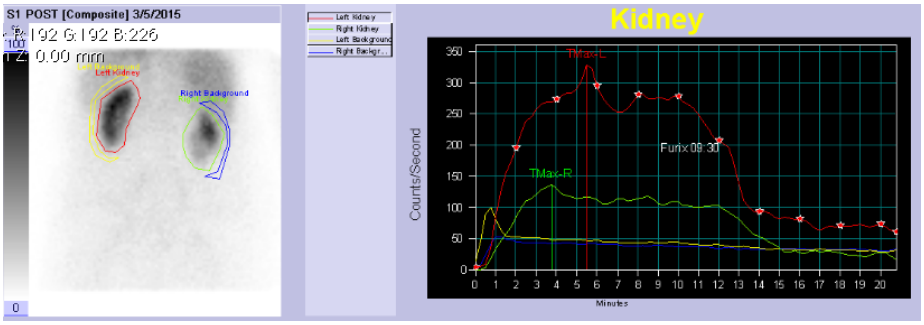

Patient 21

Images show substantial reduced kidney function on left kidney. The automatic program has a difficulty detecting boarders when kidney function is reduced.